



**University of
Zurich**
UZH

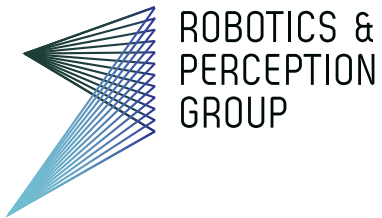
Department of Informatics



**University of
Zurich**
UZH

ETH zürich

Institute of Neuroinformatics



Ivan Alberico

Vision-Based Navigation for Mid-Air Helicopter Delivery on Mars

Master Thesis

Robotics and Perception Group
University of Zurich

Supervision

Jeff Delaune
Giovanni Cioffi
Prof. Dr. Davide Scaramuzza

October 2023

Acknowledgments

I would like to begin by expressing my deepest gratitude to Professor Dr. Davide Scaramuzza for granting me the invaluable opportunity to participate in this internship at NASA Jet Propulsion Laboratory. Without his support and belief in my abilities, I would have never embarked on this incredible journey.

Next, I would like to express my sincere appreciation to my JPL supervisor, Jeff Delaune, whose exceptional guidance has been instrumental throughout my time here. His mentorship has not only expanded my knowledge but has also provided me with valuable insights and support. Thank you for being an exceptional and approachable supervisor and for entrusting me with the opportunity to work on such an exciting project.

I would like also to extend my heartfelt gratitude to Giovanni Cioffi, supervisor from the Robotics and Perception Group, for his unwavering support from across the globe. His expertise and readiness to help me, even from afar, have profoundly enriched my internship experience, and I am genuinely appreciative of his support.

Last but certainly not least, I want to express my gratitude to the interns of the 316 Lab at JPL. Your constant support and all the constructive discussions we shared have brightened my working days and made this experience even more memorable.

Pre-Decisional Information – For Planning and Discussion Purposes Only

This research was carried out at the Jet Propulsion Laboratory, California Institute of Technology, and was sponsored by JVSRP and the National Aeronautics and Space Administration (80NM0018D0004).

Contents

Abstract	v
Nomenclature	vii
1 Introduction	1
1.1 Robotic exploration on the Red Planet	1
1.1.1 Touchdown on Mars: The Mars 2020 Mission	1
1.1.2 The next generation of Mars rotocrafts: the Mars Science Helicopter (MSH)	2
1.2 Mid-Air Helicopter Delivery (MAHD)	4
1.2.1 Benefits with respect to previous EDL strategies	4
1.2.2 Key Phases in the MAHD mission	5
1.3 Problem Statement: Navigation during the jetpack phase	5
1.4 Main challenges	6
1.5 Contributions	8
2 Literature Review	9
2.1 NASA Vision-based navigation frameworks for Mars exploration	9
2.1.1 Mars 2020 Vision-based Navigation	9
2.1.2 Navigation on the Mars Science Helicopter	10
2.2 Visual-Inertial Odometry frameworks with 1D-LRF sensors	11
3 Representative Mars Simulation Environment Development	13
3.1 Requirements for a MAHD simulation environment	13
3.2 Addressing limitations in existing drone simulators	14
3.3 Mars environment model generation from HiRISE	14
3.4 Unity integration and sensors API	15
4 Online feature initialization with 1D-LRF measurements	17
4.1 Assumptions and failure mode of xVIO	17
4.1.1 Description of the Range-Visual EKF Update	18
4.1.2 Performance degradation with range-facet model update .	19
4.2 Range-visual update without terrain local planarity assumption .	22
4.2.1 Selection criteria for range-based features	22
4.2.2 Range-features initialization	24
4.2.3 EKF SLAM update with range features	25

5 Experiments	27
5.1 Sensor noise specifications	27
5.2 Framework validation with known state initial conditions	28
5.3 Evaluation of the range-feature initialization method	30
5.3.1 Scale observability with range-feature initialization	31
5.3.2 Improved performance on MAHD trajectories	31
5.4 MAHD Monte Carlo analysis	33
5.4.1 Experimental setup	33
5.4.2 Results	34
6 Discussion	39
6.1 Conclusion	39
6.2 Future Work	40

Abstract

In the realm of Mars robotics exploration, the groundbreaking Mid-Air Helicopter Delivery (MAHD) mission concept represents a paradigm shift in Entry, Descent, and Landing (EDL), introducing a revolutionary approach to deploy drones on the Red Planet. Unlike its predecessors, MAHD leverages a jetpack to decelerate the Mars Science Helicopter (MSH) after separation from the back-shell, allowing it to achieve the ideal conditions for helicopter take-off in mid air. While the MAHD mission concept promises significant benefits, including cost reduction, access to challenging terrains, and increased payload capacity, its ambitious goals also give rise to a distinct set of challenges, particularly within the domain of monocular visual-odometry frameworks employed for the navigation of these technologies.

In this work, we conduct an extensive analysis of the range-VIO method under the challenging conditions of MAHD. The investigation takes place in a custom simulation environment designed to replicate the intricate complexities of Mars landscapes, including rough terrain with steep elevation slopes and high-altitude trajectories starting at 12 kilometers above the Martian surface. The findings from our study reveal a critical limitation in the existing range-VIO approach, particularly when applied to high altitudes and on highly non-planar terrains, where the assumption of local planarity becomes significantly violated, leading to performance degradation. To address this issue, we propose an innovative alternative to the range-VIO method that eliminates the need for any type of ground planarity assumption, making it adaptable to any terrain structure, while still being able to observe scale and mitigate error drift under constant-velocity motion and without relying on prior maps. We provide a robust evaluation of this novel implementation, demonstrating its effectiveness in a realistic simulation environment. By conducting exhaustive assessments using flight data representative of MAHD's scenarios, we highlight the potential benefits and enhanced performance of this new approach, paving the way for more adaptable and efficient navigation systems in the context of Mars exploration.

Nomenclature

Notation

${}^B\mathbf{p}_A$	translation vector from frame A to frame B
\mathbf{q}_A^B	quaternion representation of the orientation of frame A with respect to frame B
$\mathbf{C}(\mathbf{q}_A^B)$	rotation matrix representation of the orientation of frame A with respect to frame B
${}^i\mathbf{z}$	measurement at time i for Extended Kalman Filter update
$\mathbf{h}(\mathbf{x})$	non-linear measurement function for Extended Kalman Filter update
${}^A\mathbf{u}_B$	unit vector pointing to frame B and expressed with respect to frame A

Scalars are written in lower case letters (a), vectors in lower case bold letters (\mathbf{a}) and matrices in upper case bold letters (\mathbf{A}).

Acronyms and Abbreviations

VIO	Visual Inertial Odometry
EKF	Extended Kalman Filter
SLAM	Simultaneous Localization And Mapping
IMU	Inertial Measurement Unit
LRF	Laser Range Finder
MAHD	Mid-Air Helicopter Delivery
EDL	Entry, Descent and Landing
MSH	Mars Science Helicopter
LVS	Lander Vision System
MRL	Map Relative Localization
HiRISE	High Resolution Imaging Science Experiment
DTM	Digital Terrain Model
MOLA	Mars Orbiter Laser Altimeter
AGL	Above Ground Level

Chapter 1

Introduction

Over the past decades, space exploration has undergone profound transformations, thanks to the integration of robotics into its missions. These robotic systems, encompassing spacecraft and planetary rovers, have established themselves as pioneers in advancing human knowledge through their capability to navigate and interact with extraterrestrial environments. Particularly noteworthy is the emergence of aerial robots, marking a significant milestone by extending scientific reach to previously inaccessible and hazardous terrains. Among the most critical capabilities of these robots is their ability to autonomously determine their location within their surroundings. It is worth emphasizing that while state estimation for terrestrial drones often relies on GPS technology, such technologies are unavailable on other planets. Consequently, alternative sensor-based solutions, like Laser Rangefinders, must be seamlessly integrated into existing navigation frameworks to address these limitations.

1.1 Robotic exploration on the Red Planet

The Mars robotic exploration program has witnessed a remarkable evolution over the years, characterized by a shift towards increasingly ambitious missions propelled by advanced scientific objectives and cutting-edge technology. Notably, the introduction of aerial robots has refocused the interest on Martian geology and the exploration of the possibility of past life on the Red Planet. This shift encompasses the rigorous exploration for signs of historical life and meticulous preparations for forthcoming human missions. This evolution traces its roots back to the Viking Missions in the 1970s, marking the beginning of a series of successful landings on Mars. Since then, the field of robotics technology has achieved remarkable strides, ultimately culminating in outstanding achievements witnessed during the Mars 2020 mission.

1.1.1 Touchdown on Mars: The Mars 2020 Mission

The Mars 2020 mission [2] marks a significant milestone in space exploration, with particular focus on the groundbreaking achievements of the Mars Helicopter, Ingenuity. This autonomous rotorcraft, the first-ever to achieve pow-

ered, controlled flight on another planet, has expanded the mission's capabilities and scientific potential. The overarching objective of the Mars 2020 mission revolves around the comprehensive exploration and study of Mars, with a specialized emphasis on astrobiology, the quest for traces of ancient microbial life, and the meticulous collection of samples for potential return to Earth. During the crucial Entry, Descent, and Landing (EDL) phase, Perseverance employed innovative techniques, notably the "sky crane" maneuver. In this daring operation, retrorockets and a hovering descent stage were instrumental in ensuring a precise and gentle landing of the rover on the Martian surface. Notably, during this critical EDL phase, Ingenuity remained securely stowed within Perseverance to avoid any potential interference. Since then, as of October 2023, Ingenuity has triumphantly achieved 60 successful flights on Mars. While this achievement is indeed remarkable, it is essential to recognize that Ingenuity possesses limitations, particularly when it comes to exploring hazardous Martian landscapes.



Figure 1.1: The figure shows an artistic illustration of the sky-crane maneuver with Curiosity [13]. Mars 2020 descent stage with Perseverance features the same configuration.

1.1.2 The next generation of Mars rotocrafts: the Mars Science Helicopter (MSH)

The proposed Mars Science Helicopter (MSH) stands as a significant leap forward in the realm of Martian exploration, surpassing its predecessor, Ingenuity, in various aspects. The concept of MSH, first introduced in [23], includes notable features such as a hexacopter configuration equipped with six rotors, each adorned with four blades. This design ensures enhanced stability and control, vital for conducting precise scientific missions. A strategic choice was made to enable MSH to fit within the Mars heritage aeroshell's diameter, a decision driven by cost-saving measures and the wealth of experience gained from past Mars missions like Pathfinder, Mars Exploration Rover, Phoenix, and Insight.

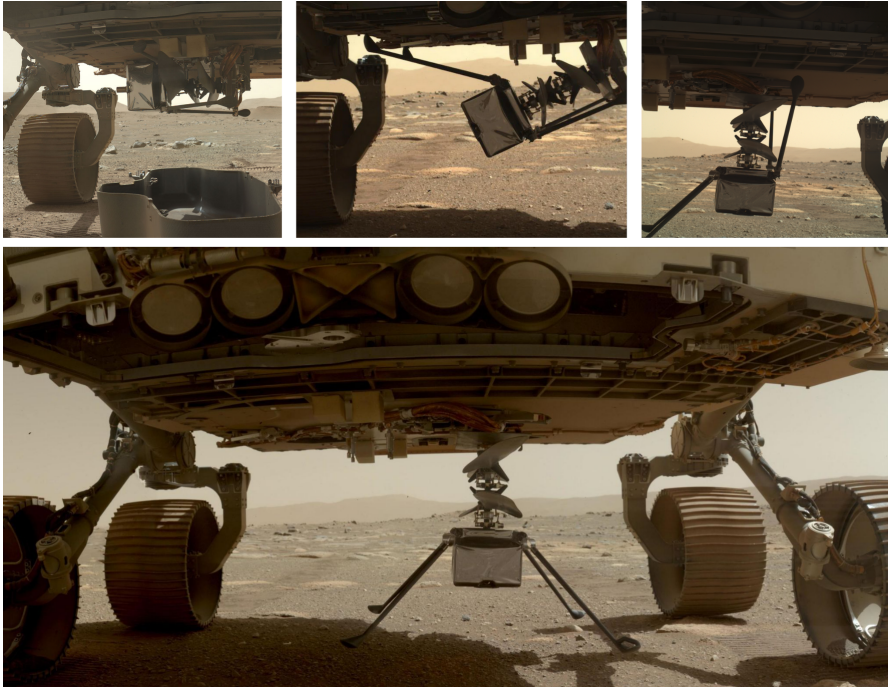


Figure 1.2: The figure shows some highlights of the deployment process of Ingenuity, which had been stowed on the underside of the Mars Perseverance rover during the EDL on Mars [15].

What truly sets MSH apart is its remarkable payload capacity, capable of transporting up to 5 kilograms of scientific payload. This expanded capability empowers MSH to conduct in-depth scientific investigations across a wide spectrum of mission objectives. Moreover, MSH exhibits impressive flight range capabilities, with the capacity to cover up to 13.3 kilometers in a single flight or hover in place for up to 6.5 minutes. This level of flexibility enables MSH to access terrains previously deemed inaccessible, such as cliffs, craters, and steep slopes, offering new avenues for scientific exploration.

Importantly, MSH plays a pivotal role in cost-effective Mars exploration by virtue of its smaller size and reduced complexity compared to traditional rovers. This streamlined approach translates into substantial cost savings throughout the mission’s development and operational phases. While rovers remain indispensable for ground-based exploration, MSH provides a complementary aerial perspective. It excels in reaching remote and challenging terrains, including high-elevation regions and hazardous areas. By achieving this, MSH enriches our scientific understanding of Mars and helps unlock the mysteries of the Red Planet.



Figure 1.3: Proposed design of the NASA Mars Science Helicopter taken from [17].

1.2 Mid-Air Helicopter Delivery (MAHD)

Mid-Air Helicopter Delivery (MAHD) [8] is an innovative Entry, Descent, and Landing system for Mars missions. It employs a jetpack to facilitate helicopter take-off after separation from the backshell, improving rotorcraft performance, simplifying architecture, reducing costs, and enabling access to challenging terrains.

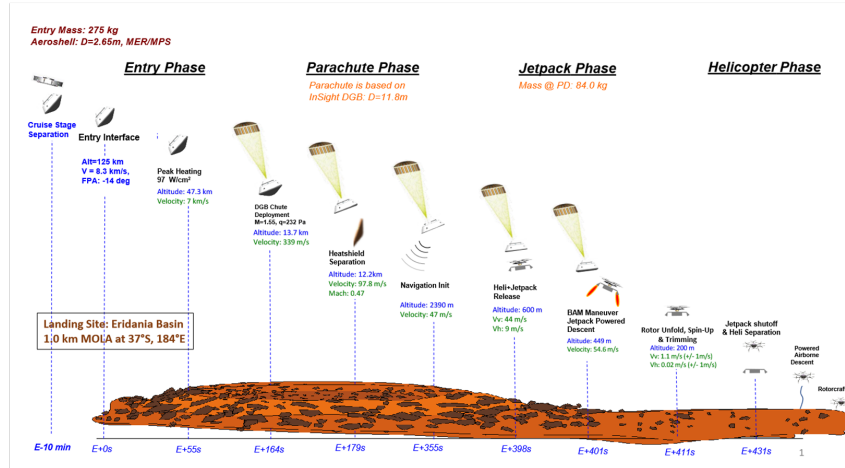


Figure 1.4: Concept of operations for the jetpack-assisted Mid-Air Helicopter Delivery system. Numbers are representative of a landing site at Eridania Basin at $L_s = 335$ deg (late Southern summer). Velocity and altitude are expressed with respect to the local terrain. [8]

1.2.1 Benefits with respect to previous EDL strategies

MAHD introduces a range of compelling advantages when compared to conventional EDL approaches. One of the standout features of MAHD is the absence of a lander. Unlike the Mars 2020 mission, which relies on the sky-crane to execute the descent, MAHD optimizes the available space within the aeroshell for larger rotorcraft. This elimination of the lander represents a significant cost reduction, making missions more economically feasible. In addition to that, MAHD simplifies the EDL system, reducing mission complexity and associated costs substantially. The streamlined architecture enhances efficiency and reliability during the critical descent and landing phases. Lastly, building upon the success of the Mars Science Helicopter, MAHD extends the reach of exploration by providing access to hazardous and higher-elevation terrains on Mars and therefore opening up new possibilities for scientific investigation. These advantages position MAHD as a highly promising EDL solution for Mars missions, particularly those focused on helicopter-only endeavors, such as the Mars Science Helicopter. MAHD not only enhances cost-effectiveness and mission feasibility but also broadens the horizons of Martian exploration by venturing into challenging terrains that were once out of reach.

1.2.2 Key Phases in the MAHD mission

A schematic representation of the main steps of the MAHD EDL can be observed in Figure 1.4. MAHD system comprises several key stages to facilitate the safe deployment and take-off of the Mars Science Helicopter:

1. **Parachute Deployment:** After the cruise stage separation, MAHD begins with the aeroshell's atmospheric entry, following a ballistic trajectory, and the subsequent deployment of the parachute, similarly to the Mars 2020 EDL procedure.
2. **Heatshield Separation:** Approximately 13.7 km kilometers above the Martian surface, the heatshield separates, marking the commencement of the navigation phase. Concurrently, the helicopter's range visual-inertial navigation system initializes.
3. **Helicopter and Jetpack Release:** At an altitude of around 600 meters above ground level (AGL), the helicopter, connected to a jetpack, separates from the backshell. Following a brief freefall, the jetpack's thrusters ignite, serving to stabilize and divert from the backshell.
4. **Rotor Wind-Trimming:** The jetpack reaches a terrain-relative hover at an altitude of 200 meters AGL, leveraging a force-torque sensor to fine-tune the helicopter's rotors, preparing for a safe take-off.
5. **Jetpack Shutoff and Helicopter Separation:** Subsequently, the helicopter deploys its rotor arms and initiates the spin-up of its rotors, readying for take-off.
6. **Helicopter Descent:** If necessary, the jetpack executes a lateral delta-V maneuver, while the helicopter adjusts the trim of its rotors for level flight. The jetpack is then detached, allowing the helicopter to commence its flight.

1.3 Problem Statement: Navigation during the jetpack phase

In the context of navigation, the main objective is to precisely control the jetpack's velocity, maintaining it within the tight boundaries of 1 m/s . This critical phase of navigation begins after heatshield separation, typically occurring at an altitude of around 12 kilometers above the Martian surface. Here, terrain-relative navigation comes into play, providing essential positional accuracy.

During this descent phase, the primary focus is on accurately estimating the vehicle's velocity, a pivotal factor for both the safe landing and the subsequent control of the jetpack in the final stages of descent. While attitude initialization is facilitated using a star tracker from orbit, velocity initialization is not feasible in the context of MAHD due to the lower accuracy of the planned IMU, as opposed to the one utilized in previous lander missions. As the Mars Science Helicopter approaches an altitude of approximately 200 meters above the Martian surface, it transitions into the terrain-relative hover phase of the jetpack.

At this juncture, having a precise estimate of the vehicle's velocity becomes paramount as it forms the basis for controlling the jetpack's operations.

To meet the stringent mission specifications, the navigation system aims to provide velocity estimates well within the 3σ bounds of 1 m/s . This level of precision is indispensable for maintaining a stable hover and facilitating a secure transition to powered flight. The $3\sigma 1\text{m/s}$ velocity MAHD specification is crucial to ensure the stability of the control feedback loop for velocity and torque control on the jetpack, which is essential for the safe and precise navigation of the helicopter during its descent and landing on Mars. However, achieving this specification can be quite challenging, considering the intricate dynamics of the jetpack and helicopter configuration and the presence of unpredictable and variable wind patterns. Notably, these wind patterns can reach velocities of up to 45 m/s (3σ), while vertical airspeed remains comparatively negligible.

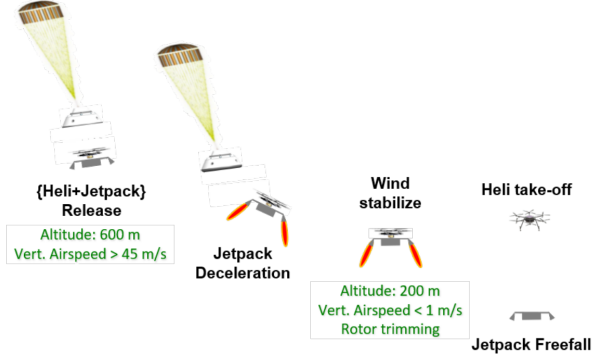


Figure 1.5: Schematic representation of the jetpack release phase [8].

1.4 Main challenges

The navigation challenges of the Mars Science Helicopter are multifaceted and intricate. First and foremost, navigating over the highly non-planar Martian terrain, exemplified by regions like Valles Marineris with its substantial altitude variations of $\pm 4 \text{ km}$, as it is shown in Figure 1.6, demands a navigation system that can swiftly adapt to changes in altitude and negotiate the rugged landscape effectively.

Secondly, the initialization of the state estimator under the uncertain and demanding conditions of MAHD is a critical concern. The prior knowledge of the helicopter's state may not suffice for achieving convergence and precise state estimation during descent, necessitating the potential implementation of an independent initialization module for the Kalman Filter.

Furthermore, MAHD encounters phases of constant velocity motion, particularly during the parachute and jetpack terrain-relative hover phases¹. The constant velocity motion in the latter two phases poses challenges for motion estimation, as it lacks the IMU sensor excitations observed in more dynamic maneuvers. The work done in [7], [24] and [16], shows that scale observability becomes a major concern under conditions of constant-velocity motion, as scale error leads to position and velocity drift that can drastically affect navigation performance. To address this, integrating additional sensors like altimeters becomes imperative to disambiguate scale information.

Lastly, MAHD conducts terrain-relative navigation without access to prior maps of the Martian surface. Instead, it relies on continuous comparisons of sensor data with observed terrain features in real-time. While this approach enables the system to determine its position and orientation relative to the local terrain, it cannot correct x and y position errors in an absolute sense, only relative to the initial guess fed into the state estimation framework. This meticulous focus on maintaining position accuracy relative to the immediate surroundings is vital for safe navigation through the Martian terrain and achieving a precise landing. These challenges collectively underscore the complexity of navigation for MAHD.

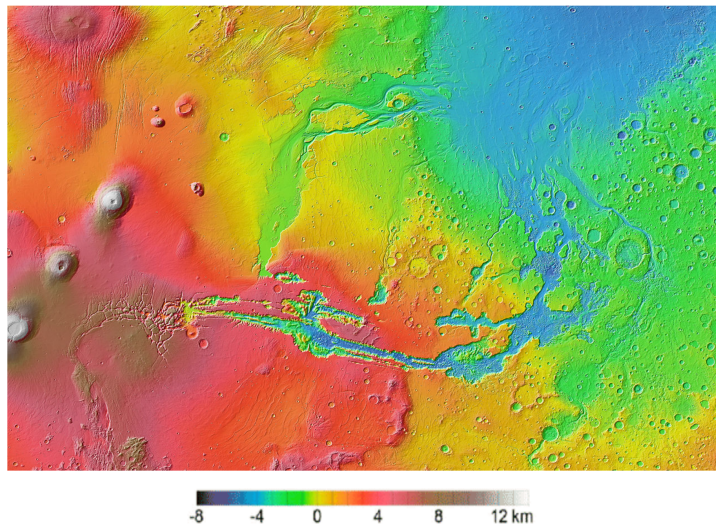


Figure 1.6: Elevation map of Valles Marineris. The elevation heat map shows that some areas in the site present abrupt changes in elevation, going from -4 to $+4$ km measured from the Mars Orbiter Laser Altimeter (MOLA) [21].

¹The primary goal of the parachute phase is to gradually decelerate the MSH and the jetpack system until they reach a state of zero acceleration. This is achieved through the deployment of a specially designed parachute, which generates drag forces exceeding gravitational acceleration, ensuring a controlled descent and setting the stage for subsequent phases. As for the jetpack terrain-relative hover during rotors' trimming, the system's motion is constrained to near-zero velocity and zero acceleration just before the jetpack's release. Achieving and maintaining near-zero velocity is crucial, as any drift in the estimated state, if not corrected, can lead to navigation inaccuracies and impact the landing's precision.

1.5 Contributions

The main contributions are the following:

1. **Development of a Simulation Environment representative of Mars:**
A significant contribution of this work is the creation of a photorealistic and highly representative simulation environment replicating the Mars surface. This simulation environment possesses the capability to accurately reproduce the challenging conditions associated with Mid-Air Helicopter Delivery. These conditions encompass 3D terrains characterized by steep elevation slopes, offering a critical testbed for MAHD simulations. Furthermore, the simulation environment is intended to simulate constant velocity trajectories at high altitudes, allowing for a comprehensive assessment of MAHD under various stress cases.
2. **Performance assessment of MSH Visual-Odometry framework:**
A pivotal facet of the thesis revolves around the comprehensive evaluation of the proposed Range-Visual-Inertial-Odometry framework (xVIO) that will operate on the Mars Science Helicopter. This assessment is conducted by evaluating the framework to MAHD-like trajectories generated within the developed simulation environment. By rigorously testing xVIO under the demanding conditions described in Section 1.4, the thesis provides valuable insights into its performance and robustness. Extensive testing revealed that an independent initialization module is unnecessary. A significant contribution of this work is demonstrating that, within the context of EKF, there is no need for independent initialization due to the low velocity-to-altitude ratio and minimal attitude propagation since entry. This evaluation serves as a critical step in ensuring the viability of xVIO for MSH navigation.
3. **Novel algorithm for Laser Range Finder integration without planarity assumption:** The thesis introduces a novel algorithm that seamlessly integrates Laser Range Finder measurements within the xVIO framework, all without relying on the assumption of local planarity of the terrain. This innovation opens new avenues for terrain-relative navigation in complex Martian terrains, contributing to enhanced localization accuracy and reducing the reliance on assumptions that may not hold in the challenging Martian landscape.

These contributions collectively advance our understanding of robotic navigation in Mars-like environments, addressing critical challenges and paving the way for more robust and capable robotic systems for future space exploration missions.

Chapter 2

Literature Review

In the context of MAHD, the significance of incorporating altimeter measurements for scale observation cannot be overstated, as previously highlighted in Chapter 1. The challenge arises when navigating constant velocity trajectories during the parachute and the jetpack hovering phases of the MAHD EDL. Contemporary state-of-the-art monocular visual-odometry algorithms that integrate altimeter data typically make ground plane assumptions, whether applied globally or locally to the scene. This characteristic is shared by algorithms employed by NASA for missions like Mars 2020 as well as those commonly featured in academic research.

2.1 NASA Vision-based navigation frameworks for Mars exploration

This section will provide an overview of the state-of-the-art vision-based navigation frameworks utilized by NASA. Firstly, we will go over the frameworks employed during EDL and on Ingenuity in the context of Mars 2020 mission. Subsequently, we will shift the focus to the framework selected for employment on the MSH for research concepts like MAHD.

2.1.1 Mars 2020 Vision-based Navigation

The Lander Vision System (LVS) [12] is a navigation framework integrated into Mars 2020 to reduce the position error down to 40 meters with respect to a predefined landing site map. Without the use of LVS, the errors in position can be as large as 3.2 kilometers, highlighting its crucial role in avoiding potential hazards and ensuring a safer landing on Mars. LVS operates within the framework of Map Relative Localization algorithms, which involve the fusion of landmark matches extracted from descent images with data from an inertial measurement unit. However, one of the primary limitations of this algorithm becomes evident in its dependence on a prior map for state estimation. In addition to introducing an additional dependency to the entire pipeline, it can also become a limiting factor during descent, particularly in situations where a

map may not be accessible at the landing site. Additionally, LVS relies on full-image alignment methods, such as Fast Fourier Transform or spatial correlation, to compute landmark matches. While these methods are computationally efficient, they come with a significant drawback. They assume the terrain to be flat across the entire field of view. This assumption poses a challenge, particularly in terrains with high non-planar features, as encountered in the context of MAHD. Consequently, these limitations make LVS less suitable for the employment in such challenging environments.

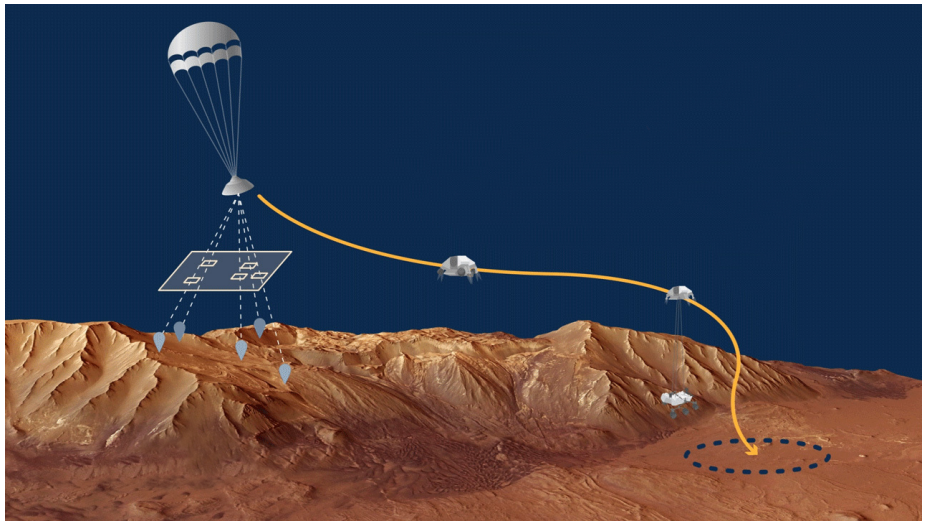


Figure 2.1: This animation illustrates the Terrain-Relative Navigation technique (LVS) integrated into the EDL process for the Mars 2020 rover. As it descends, the rover captures images of the surface, enabling rapid assessment of its trajectory relative to predetermined hazardous areas within the landing zone. When necessary, the rover can execute a divert maneuver to redirect its path towards safer terrain [14].

Another notable framework employed in the Mars 2020 mission, particularly for NASA’s Ingenuity Mars Helicopter navigation, is described in [1]. This framework introduces a range-visual-inertial odometry algorithm that cleverly integrates Laser Range Finder measurements to enable scale observation. An interesting feature of this approach is its ability to maintain a relatively low-dimensional estimator with just 21 states. However, this efficiency comes with a trade-off, as it hinges on the assumption that the observed scene is flat. While this assumption may be suitable for specific applications, it may not be universally compatible with the diverse and often non-planar terrains encountered in various robotics scenarios. This framework, though valuable, highlights the need for adaptability when addressing scale observation in different terrain contexts.

2.1.2 Navigation on the Mars Science Helicopter

The envisioned navigation framework for the proposed Mars Science Helicopter during its MAHD operations is detailed in [7] and is referred to as xVIO. This framework is a sophisticated vision-based navigation system that is going to

serve a dual role during the MAHD mission concept: it is expected to operate during the EDL phase and also to be used for autonomous navigation on Mars. The Visual-Inertial Odometry system relies on an Extended Kalman Filter for its state estimation process, leveraging visual measurements to constrain the EKF's inertial propagation. Each feature match serves as a measurement that plays a crucial role in refining and updating the drone's state estimate, after being parameterized relative to the anchor camera pose where it was initially observed. The primary strength of xVIO becomes evident in scenarios where there is no IMU excitation, such as constant velocity motion or hovering. This framework excels in such situations because it incorporates a range measurement model that effectively prevents VIO scale drift and adapts seamlessly to varying scene structures. The previous benefits are achieved by introducing an innovative range measurement update model based on facet constraints, that allows scale observability under different types of terrain. However, when applied in the context of MAHD, xVIO encounters certain limitations. Its main constraint stems from the assumption of local planarity in the facet model. This assumption may become more violated at higher altitudes and in scenarios featuring highly non-planar terrain, potentially affecting the algorithm's accuracy and overall performance.

A more comprehensive examination of the limitations associated with the range facet model update in MAHD conditions will be provided in Chapter 4, offering a detailed insight into the challenges faced by the xVIO framework in this specific context.

2.2 Visual-Inertial Odometry frameworks with 1D-LRF sensors

In this section, we will provide an overview of the cutting-edge vision-based navigation frameworks that incorporate Laser Range Finder data in conjunction with visual and inertial data to enhance performance and enable accurate scale estimation. Various approaches are employed to achieve this integration, and we will explore these methodologies in detail.

The method discussed in [9] features a downward-facing LRF aimed at enhancing the visual-inertial odometry state estimation. It does so by employing an Extended Kalman Filter structure, which enables the incorporation of range measurements from a single-beam Laser Range Finder and facilitates the estimation of IMU bias. In this approach, the state space is expanded to include a parameter representing the distance from the ground. The LRF data is then employed as a measurement for this particular state, which significantly enhances the localization and motion estimation process. However, it is important to note that this method relies on the assumption of a flat ground plane when modeling the distance-from-ground state in the EKF update. This assumption has the potential to limit the method's adaptability to terrains that extend beyond flat surfaces.

A different approach is the one followed in [11]. This paper introduces a novel topographic Simultaneous Localization and Mapping algorithm that relies on a single altimeter sensor. The key feature of this algorithm is its utilization of a

rectangular panel map structure, employing bilinear interpolation to represent undulating terrain. This approach simplifies the SLAM problem by reducing the map state estimation relative to observations. However, despite its innovative nature, it is important to note a limitation of this approach in the context of MAHD. The altimeter update for terrain map estimation assumes planarity within the panel being updated. This assumption makes the method unsuitable for MAHD’s application, where terrain can be highly non-planar and we are navigating at altitudes as high as 12 km.

In the work done by [22], a novel Range and Event-Based Visual-Inertial Odometry (REVIO) is presented. The proposed framework is designed to enhance localization in highly dynamic environments characterized by high-speed movements and rapid changes in brightness, leveraging the outstanding capabilities of event cameras and fusing them with range information coming from LRF sensors. Also in this case, in the process of using range information to perform a correction update, they assume that all feature points lie on the same horizontal plane, and the range information represents the distance from the sensor to that plane. The planarity assumption underscores a limitation that leads us to consider discarding this method for potential application in the context MAHD.

This work operates at the intersection between engineering and research, striking a delicate balance between leveraging established solutions for reliability and forging new paths to tackle novel challenges. On one hand, we prioritize the robustness of MAHD’s application by testing existing methodologies and drawing from the wealth of prior knowledge. On the other hand, the evolving spectrum of challenges demands exploration of novel approaches.

In this thesis, we delve into a critical problem: the observation of scale in VIO under the constraints of constant-velocity motion across any scene structures. To the best of our knowledge, no VIO method currently available offers a means to incorporate Laser Range Finder measurements without necessitating assumptions about the terrain type. This is where the proposed method takes center stage, introducing an entirely novel approach that transcends these limitations and opens up new possibilities in the field. Notably, this adaptability shines through in the context of MAHD. What sets this novel approach apart is its ability to achieve these objectives without any prior knowledge of the surrounding environment, marking a departure from previous EDL methods.

Chapter 3

Representative Mars Simulation Environment Development

One of the contributions of this work lies in the development of a highly sophisticated and comprehensive simulation environment tailored specifically for Mid-Air Helicopter Delivery operations on Mars. The importance of such a simulation environment cannot be overstated, as it serves as a fundamental tool for advancing our understanding in this unique and challenging field of planetary exploration.

3.1 Requirements for a MAHD simulation environment

In the context of this project, it is important to clarify that the primary objective is the evaluation of navigation strategies under specific conditions, rather than replicating the full spectrum of Mid-Air Helicopter Delivery complexities. Specifically, we are concerned with analyzing navigation in simple, straight-line trajectories characterized by constant drone velocity, which represent the most limiting cases for monocular visual odometry frameworks in the context of MAHD. To ensure a reliable assessment of the proposed algorithm under MAHD conditions, the following requirements are essential:

1. We require a rendering engine capable of generating images from high-precision 3D models up to distances of 12 kilometers. Visual and terrain fidelity are crucial aspects of this rendering process.
2. A comprehensive sensor suite is essential for collecting data during simulations. This suite should be capable of logging ground truth pose, IMU data, and altimeter measurements with a high degree of accuracy. These measurements should be captured while the drone follows constant velocity trajectories.

The research primarily focuses on assessing navigation performance across a broad altitude range, spanning from 12 kilometers down to 200 meters. The key emphasis is on visual and terrain fidelity, and we are particularly interested in evaluating how well Visual-Inertial Odometry algorithms can handle straight-line trajectories at constant velocity. This research scope prioritizes these specific conditions as they present unique challenges, and addressing them successfully would pave the way for more complex scenarios.

3.2 Addressing limitations in existing drone simulators

Existing drone simulators, such as Airsim [19] or Flightmare [20], pose limitations when it comes to precisely simulating the specific MAHD requirements. For example, in the previous two cases the path-following process cannot be always fully decoupled from the drone's dynamics at every timestamp of the trajectory. More specifically, making a drone follow a constant-velocity trajectory starting from an idle configuration is not possible without having the IMU register some level of excitation, due to the fact that according to the drone's dynamics we need some acceleration to start moving. Hence, it is not possible to achieve pure constant-velocity trajectories under these conditions without inducing any form of excitation in the IMU.

While simulators like Airsim, offer a way to overcome this problem, for example with the *Computer Vision* mode that allows to disable the physics engine of a drone model during the path-following, this in turn comes with other limitations. In this mode, the simulator may decouple the path-following process from the drone's dynamics, however the sensors' APIs are often unsupported in this mode, therefore it is not possible to log IMU and altimeter measurements. Hence, the need for a hybrid simulator arises from these unique requirements and limitations.

3.3 Mars environment model generation from HiRISE

In order to achieve the highest level of precision in the novel simulation environment, we use Digital Terrain Models (DTMs) of various Martian sites sourced from the High-Resolution Imaging Science Experiment (HiRISE) website. HiRISE data are derived from measurements taken by an orbiting spacecraft equipped with a powerful camera capable of capturing images covering extensive Martian terrain while discerning features with a resolution of about 1 meter.

The process begins with the integration of DTMs into Blender, facilitated by a specialized add-on tailored for HiRISE DTM integration. Within Blender, these DTMs are then converted into .fbx files, a format that aligns with Unity, which is the chosen simulation engine. Upon importing the .fbx 3D models into Unity, we overlay the corresponding texture images onto them. An example of 3D model rendered in Unity representing a site in Valles Marineris can be

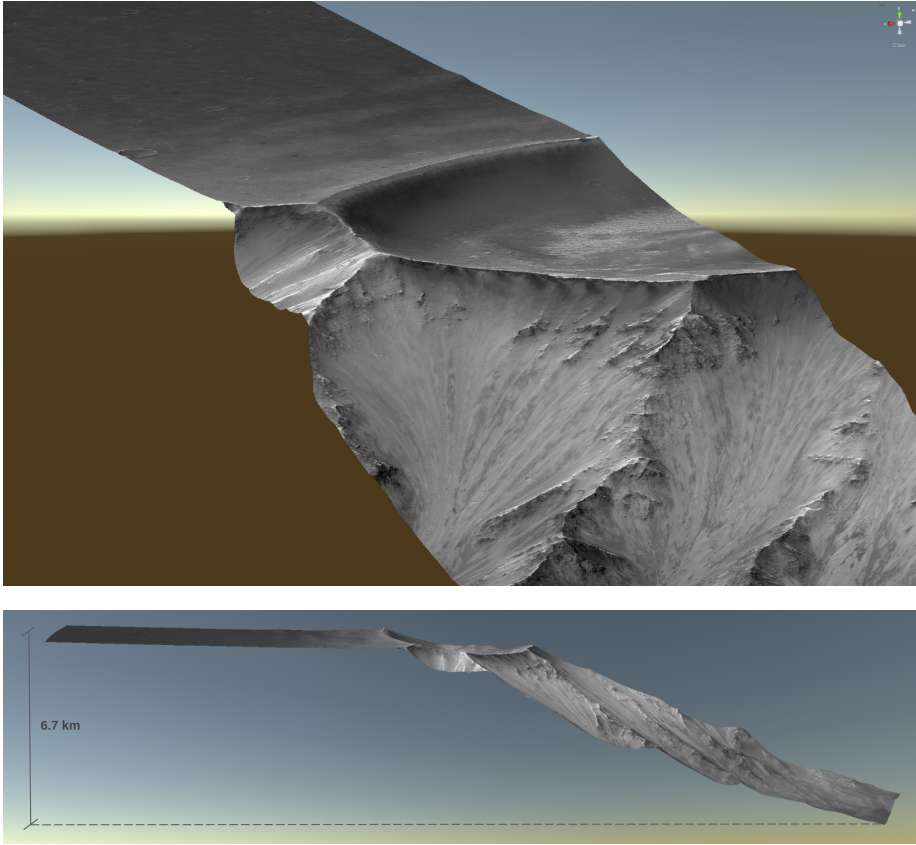


Figure 3.1: 3D model rendering on Unity of a site in Valles Marineris from HiRISE DTM. The bottom picture shows a lateral view of the model, highlighting the terrain elevation difference of roughly 6.7 km.

seen in Figure 3.1. However, in order to maintain consistency and avoid artifacts stemming from rendering images at different heights, we must deactivate certain post-processing effects. These effects, including anti-aliasing, auto exposure, motion blur, and color adjustments, can significantly impact the performance of the tracking algorithm. Given that we track features from a starting distance of 12 km, even minor errors in pixel measurements could result in significant position inaccuracies, making the deactivation of these effects essential for this research.

3.4 Unity integration and sensors API

The complete functionality of the proposed hybrid simulator is achieved through a series of key steps. Firstly, we have seamlessly integrated an external trajectory generator package with Unity, namely the Robotics Toolbox [6] package, allowing us to dynamically control the drone's position and orientation within the rendering engine over time. IMU data generation is then carried out offline, synchronized with the input trajectory provided to the rendering engine. For im-

age generation, we make use of pre-existing pinhole camera models within Unity, configured to have a downward perspective, and Airsim is employed through an existing Python API for image capture. Additionally, we have implemented a C# model for an altimeter sensor, emulating a downward-facing 1D-LRF, which employs ray-tracing techniques on the rendered 3D model to determine the distance between the drone and the ground. To manage the altimeter data collected from Unity, we have developed a dedicated Python API.

The proposed simulation environment effectively addresses the limitations found in other simulators by decoupling the drone model's dynamics from the rendering engine, and at the same time providing a way to retrieve the sensor information by means of alternative packages that are independent from the physical model of an aircraft.

Chapter 4

Online feature initialization with 1D-LRF measurements

In this chapter, we delve into the primary contribution of this thesis, which revolves around the integration of 1D Laser Range Finder measurements into the visual-odometry framework employed by the Mars Science Helicopter, denoted as xVIO. What sets this method apart is its capacity to perform this integration without necessitating any assumptions regarding the terrain's planarity. The chapter begins by showing the constraints and limitations of the range-facet model update when applied under conditions of high altitudes and extremely non-planar terrain. Subsequently, it introduces the innovative and novel method that overcomes these limitations, which guarantees improved performance in the realm of MSH navigation.

4.1 Assumptions and failure mode of xVIO

The range-facet model update in xVIO begins with a Delaunay triangulation of all SLAM features used for the visual update. This triangulation subdivides the region defined by these features into triangles or facets. The triangle that contains the Laser Range Finder measurement is selected for the update. It is worth pointing out that the assumption introduced by range-facet update has a certain degree of variability depending on the number of SLAM features we consider during VIO: with only three SLAM features, it assumes the entire world to be flat, while tracking every pixel in the image would eliminate the planarity assumptions entirely. However, practical run-time limitations make it realistic to use no more than 15 – 20 SLAM features as a compromise.

Under these computational limitations, the update relies on the assumption that the facet containing the LRF measurement represents a planar region of the terrain. Therefore, the method underlines a local planarity assumption in its practical application.

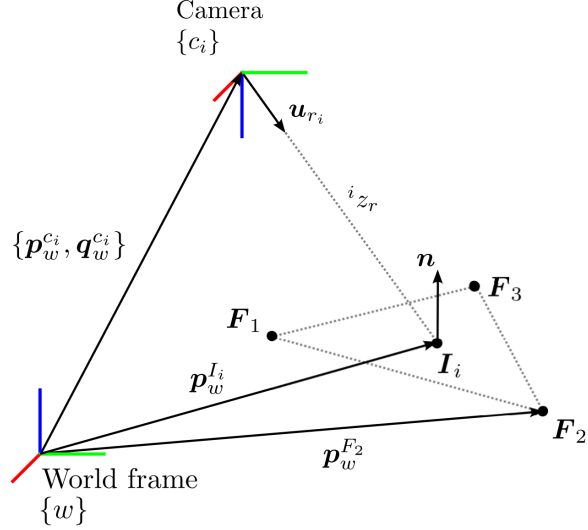


Figure 4.1: From [7], geometry of the range measurement ${}^i z_r$ at time i . F_1 , F_2 and F_3 are three SLAM features in the scene. u_{r_i} is the unit vector oriented along the measurement axis of the LRF, which is assumed to have the same origin as the camera frame c_i . I_i is the intersection point of this axis with the scene.

4.1.1 Description of the Range-Visual EKF Update

In this section, we will provide a step-by-step explanation of how the range measurement update is constructed, elucidating the formulation process. Being ${}^w u_{r_i}$ the unit vector oriented along the optical axis of the LRF at time i with respect to the world frame and ${}^w n$ the normal vector to the plane containing p_{j_1} , p_{j_2} and p_{j_3} , expressed as follows

$${}^w n = (p_w^{F_{j_1}} - p_w^{F_{j_2}}) \times (p_w^{F_{j_3}} - p_w^{F_{j_2}}) \quad (4.1)$$

If ${}^w u_{r_i} {}^T {}^w n \neq 0$, we can express the range measurement at time i as follows

$${}^i z_r = {}^i z_r \frac{{}^w u_{r_i} {}^T {}^w n}{({}^w u_{r_i} {}^T {}^w n)} = \frac{(p_w^I - p_w^{c_i}) {}^T {}^w n}{{}^w u_{r_i} {}^T {}^w n} = \frac{(p_w^I - p_w^{F_{j_2}} + p_w^{F_{j_2}} - p_w^{c_i}) {}^T {}^w n}{{}^w u_{r_i} {}^T {}^w n} \quad (4.2)$$

$${}^i z_r = \frac{(p_w^{F_{j_2}} - p_w^{c_i}) {}^T {}^w n}{{}^w u_{r_i} {}^T {}^w n} \quad (4.3)$$

The previous steps show that the range measurement model is a nonlinear function of the state, so it can be linearized to update the EKF.

$${}^i z_r = \mathbf{h}_r(x) + {}^i n_r \quad (4.4)$$

The primary challenge associated with this approach in the context of MAHD arises when operating at high altitudes and on non-planar terrains. In such conditions, there is an increased likelihood that the local planar assumption, which is essential for the facet-based model, will be violated. This means that the region encompassed by the facet may extend over a terrain area that is far from being planar. Consequently, this can lead to a higher degree of error being introduced into the navigation pipeline, ultimately resulting in a degraded performance of the state estimator. Overcoming this challenge will be a key focus for future research and development in the field.

4.1.2 Performance degradation with range-facet model update

To validate the previous hypothesis, xVIO with range-facet update has been evaluated on a MAHD sequence generated with the image-based Unity simulation environment on a terrain presenting a height variation of at most $6.7km$, specifically the one shown in Figure 3.1. The evaluation results revealed that the xVIO exhibited significantly high error values and inconsistency throughout a substantial portion of the trajectory, as illustrated in Figure 4.4b.

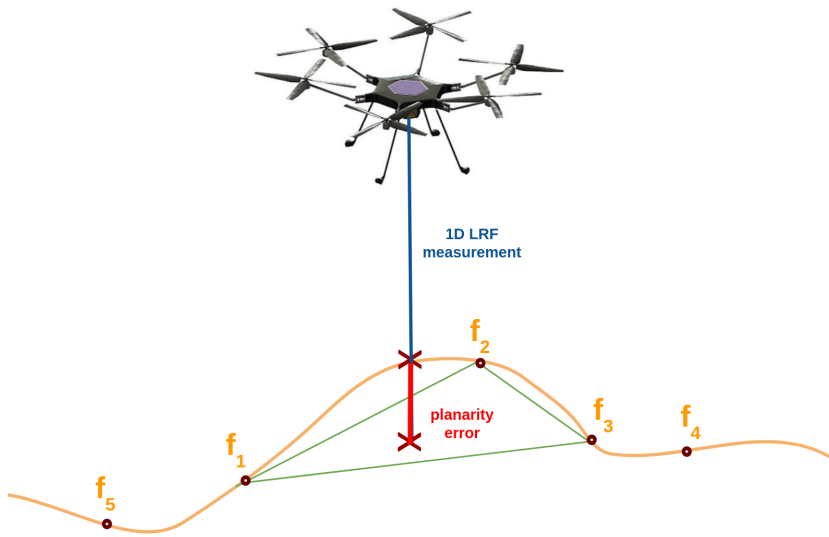


Figure 4.2: Schematic representation of the local planarity terrain assumption violation.

To validate this assumption we plot the error between the true value of the range and the projected height of the planar facet (computed with the ground truth depth of the features forming the facet). The plots in Figure 4.4a show a comparison between (a) performance of xVIO with visual update only (b) performance of xVIO with range-visual update with facet model and (c) the generated plot of the aforementioned error metrics. By setting side by side the 3 figures, it is possible to spot some correlation in the curves behavior.

The effect of the range-facet update is twofold:

- it amplifies in magnitude the error already introduced by the SLAM features update
- it introduces additional performance degradation due to larger error differences between true value of range and height of the planar facet.

By examining the two images presented in Figure 4.3 and subsequently comparing them to Figure 4.4c, 4.4b, 4.4a, it becomes evident that there is a clear correlation between the performance degradation observed in the evaluation plot of the range-facet model update and the error plot of the violation of the planarity assumption in the terrain. As we begin to traverse the crater horizontally and experience conditions where the central Delaunay triangle in which the LRF measurement occurs no longer matches to a planar surface, we notice a gradual decline in performance. As we continuously carry out an EKF update with significantly erroneous values, the state estimator's performance gradually deteriorates over time, eventually leading to inconsistent behavior and divergence. This observation underscores the impact of terrain non-planarity on the estimator's performance and highlights the need for a more robust approach in such challenging environments.

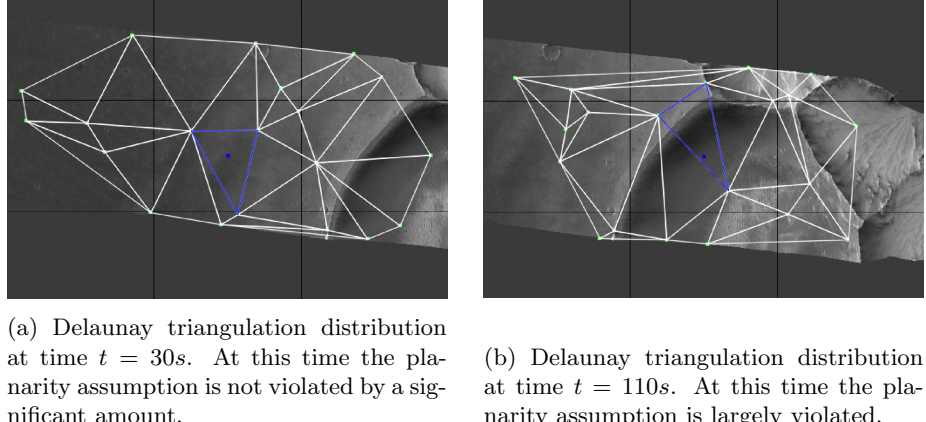
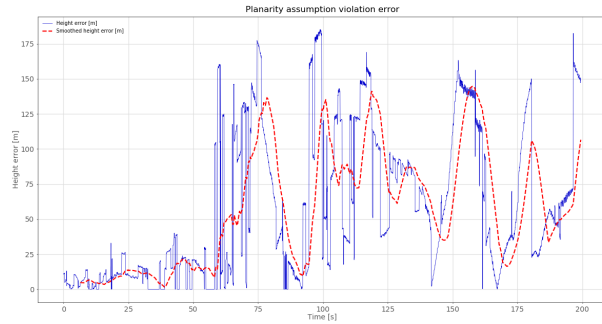
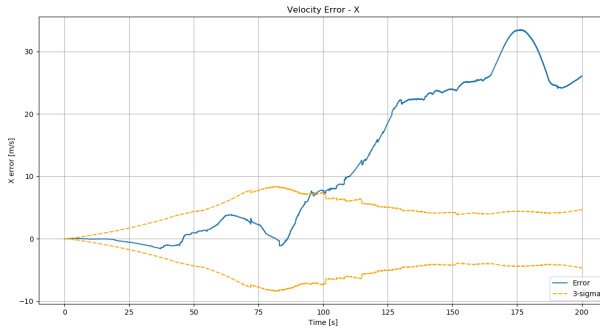


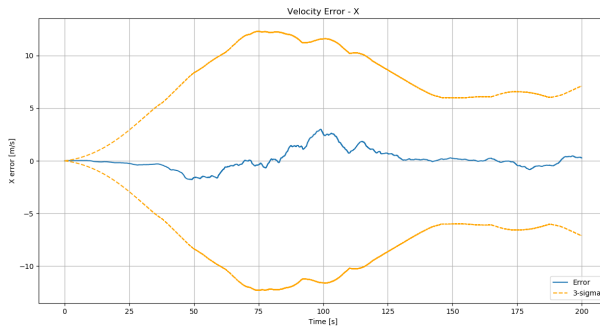
Figure 4.3: Comparison between the Delaunay triangulation distributions at two timestamps of a trajectory. The plots are representative of two moments of the trajectory in which (a) the planarity assumption is respected (b) the planarity assumption start being violated.



(a) Plot of the error between range measurement and projected height of the plane spanned by the facet used for the EKF range update. The real error is overlapped with a moving average smoothed version that is more representative of the trend.



(b) Position error on X axis of xVIO with range-facet update evaluated on a MAHD trajectory.



(c) Position error on X axis of xVIO with SLAM features update evaluated on a MAHD trajectory.

Figure 4.4: Comparison between (a) error between true altimeter value and projected height of the facet plane (b) performance of xVIO with range-facet update (c) performance of xVIO with SLAM features update only

4.2 Range-visual update without terrain local planarity assumption

This section presents a pioneering approach to incorporate altimeter readings into xVIO without relying on any assumptions about the terrain. This novel integration of altimeter data stands as the primary contribution of this work. This section is structured into three distinct segments, each addressing a crucial aspect of the range-feature integration in the context of the proposed approach. Initially, we will delve into the criteria governing the selection of new range-features. Subsequently, we will explore the comprehensive process of initializing these range-features, including an additional subsection detailing an innovative method for initializing also the other SLAM features based on LRF measurements. Finally, we will meticulously outline the primary steps involved in the Extended Kalman Filter SLAM update, emphasizing its relevance within the realm of range-feature integration.

4.2.1 Selection criteria for range-based features

Before adding a range-feature to the SLAM tracks for the visual update, we have to make sure that the feature represents a corner and that it can be tracked over time. In order to determine that, we make use of the minimum eigenvalue score metrics defined in [3], which is also used in the Pyramidal feature tracking implementation of the OpenCV Lucas-Kanade optical flow. The metrics computes the minimum eigenvalue of the spatial gradient matrix. Given an image $I(x, y)$ and its image derivatives $I_x(x, y)$ and $I_y(x, y)$, the spatial gradient matrix defined in a windows of size $[-w_x, w_x] \times [-w_y, w_y]$ around an image point of coordinates (x_{LRF}, y_{LRF}) is defined as follows

$$G = \sum_{x=x_{LRF}-w_x}^{x_{LRF}+w_x} \sum_{y=y_{LRF}-w_y}^{y_{LRF}+w_y} \nabla I \nabla I^T = \sum_{x=x_{LRF}-w_x}^{x_{LRF}+w_x} \sum_{y=y_{LRF}-w_y}^{y_{LRF}+w_y} \begin{bmatrix} I_x^2 & I_x I_y \\ I_x I_y & I_y^2 \end{bmatrix} \quad (4.5)$$

The metrics is defined as the minimum eigenvalue of matrix G . For this specific case, the score is computed for the central pixel at every iteration. A new range-feature is determined when both of the following conditions are satisfied:

1. The minimum eigenvalue score is above a predefined threshold;
2. The score value at time t is greater than the score computed in the subsequent N iterations, with N being a parameter specified at run-time.

Condition (1) serves the purpose of selecting good features to track, aiming to focus the attention on image points exhibiting substantial variations in intensity or texture, such as corners. By filtering out points with low eigenvalues, we effectively prioritize features that are more likely to yield meaningful information.

Condition (2) is crucial for determining the optimal pixel within a time window of size N within the trajectory. As illustrated in Figure 4.5, desirable features to track align with the peaks in the curve. However, in practical scenarios,

we assess the score of the central pixel iteratively in real-time, and we cannot predict precisely when the peak will occur. By establishing this criterion, we ensure that the pixel we select as a range-feature is likely to be a peak because the subsequent N measurements consistently yield lower values. Using too small an N might lead us to select local maxima of the score function, as corners do not always exhibit strictly increasing or decreasing scores. Conversely, overly large values of N might cause us to overlook certain corners along the way, especially when two peaks are closely spaced.

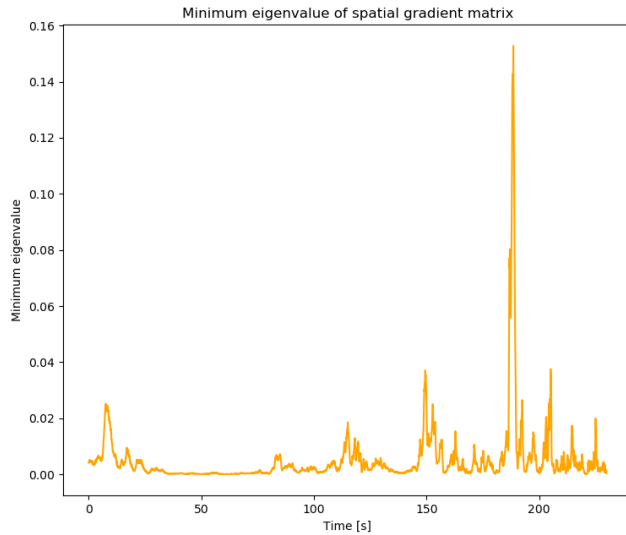


Figure 4.5: Minimum eigenvalue of the spatial gradient matrix computed in a 9×9 window around the central pixel of coordinates $(x, y) = (320, 240)$.

Moreover, to further refine this selection process, we have implemented a time-out mechanism for triggering consecutive range-features. This measure prevents the inclusion of highly similar features in the update, ensuring diversity and robustness in the selection of range-features.

The plot in Figure 4.5 shows the minimum eigenvalue linked to the central pixel within a 9×9 window across a trajectory within the MAHD context. Notably, distinct peaks are discernible in the plot, each corresponding to favorable features suitable for tracking. Taking into account the insights derived from this plot and following a comprehensive examination across various trajectories, we have arrived at the determination that an optimal threshold value for the selection of viable range-features to be tracked is $T = 0.01$. This threshold value has demonstrated its effectiveness in reliably identifying and tracking the most suitable features throughout different scenarios and trajectories in the MAHD context. However, one could consider lowering this threshold in conditions of poor texture of the environment.

4.2.2 Range-features initialization

Once a pixel satisfies the conditions elucidated in the preceding section, it becomes a candidate for inclusion in the feature matches and subsequently undergoes tracking, following a protocol similar to that of any other SLAM feature. As it persists in being tracked for a duration exceeding the minimum track length parameter specified at run-time, it attains eligibility for inclusion in the set of SLAM tracks used for updates. What sets it apart from the other SLAM tracks is the intentional effort to guarantee the inclusion of the range-feature within these tracks, and additionally the way these features are initialized.

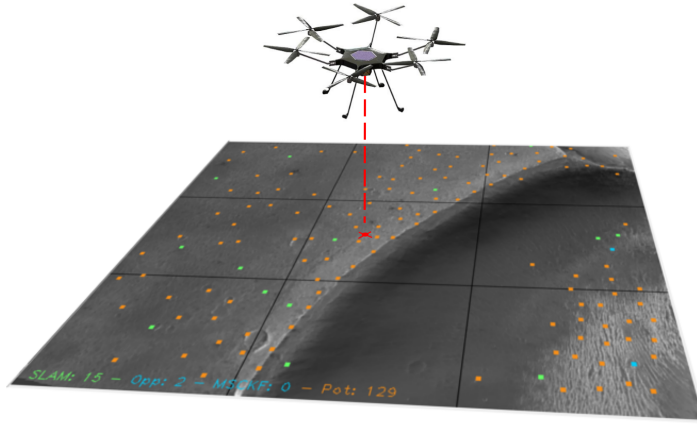


Figure 4.6: Visual representation of the range-feature initialization method.

The feature state associated with the new range-feature

$$\mathbf{f}_{LRF_j} = [\alpha_{LRF_j}, \beta_{LRF_j}, \rho_{LRF_j}]^T \quad (4.6)$$

represents the *inverse-depth parameterization*¹ of the measurement ${}^{c_i}p_{LRF_j}$ expressed with respect to camera frame c_i at time i . Being ${}^i\tilde{z}_r$ the value the altimeter measures at time i , the initial inverse-depth estimate of the new feature is set to $\hat{\rho}_{0_{LRF_j}} = \frac{1}{i}\tilde{z}_r$, with the corresponding standard deviation $\sigma_{0_{LRF_j}}$ being initialized with the standard deviation of the Laser Range Finder model used in practice. Whenever a new range-feature is being tracked, the state space estimate is augmented in the following way

$$\hat{x}_{aug_{k|k}} \leftarrow \begin{bmatrix} \hat{x}_{k|k} \\ \hat{\alpha}_{0_{LRF_j}} \\ \hat{\beta}_{0_{LRF_j}} \\ \hat{\rho}_{0_{LRF_j}} \end{bmatrix} \quad (4.7)$$

¹The inverse-depth parameterization has been used to represent feature coordinates in SLAM due to its improved depth convergence properties [4].

SLAM features initialization with 1D-LRF measurements

The default implementation of xVIO performs dynamic feature initialization of the inverse feature depth of the SLAM features by defining a plane and computing the distance of the drone to that plane at the timestamp at which the features are being initialized. As this method is very sensitive to the current estimate of the drone state and also to bad initialization of the position, a new feature initialization method is proposed, which instead initializes the inverse depth based on the altimeter measurement at that timestamp. We set $\hat{\rho}_0 = \frac{1}{^i\tilde{z}_r}$ and $\sigma_{\rho_0} = \frac{1}{2\hat{\rho}_0}$, with $^i\tilde{z}_r$ being the measurement of the altimeter at time i . According to [5], setting the previous value of σ_{ρ_0} defines a 95% confidence region for the depth in the interval

$$\left[\frac{1}{\hat{\rho}_0 - 2\sigma_{\rho_0}}, \frac{1}{\hat{\rho}_0 + 2\sigma_{\rho_0}} \right] \quad (4.8)$$

Similarly to (4.7), whenever a new SLAM feature p_j is being tracked, the state space estimate and error covariance matrix are augmented as follows

$$\hat{x}_{aug_{k|k}} \leftarrow \begin{bmatrix} \hat{x}_{k|k} \\ \hat{\alpha}_{0j} \\ \hat{\beta}_{0j} \\ \hat{\rho}_0 \end{bmatrix} \quad (4.9)$$

$$P_{aug_{k|k}} \leftarrow \begin{bmatrix} P_{k|k} & 0 & 0 \\ 0 & \sigma_V^2 I_2 & 0 \\ 0 & 0 & \sigma_{\rho_0} \end{bmatrix} \quad (4.10)$$

with σ_V being the standard deviation of the normalized image feature noise.

4.2.3 EKF SLAM update with range features

Once the range feature has been added to the SLAM tracks, the update rule for that feature follows the same pattern of any other SLAM feature. As it is defined in [7], being z_j the image measurement of feature p_j observed in camera c_i in the normalized plane $^{c_i}z = 1$, the measurement model for the SLAM visual update can be expressed as follows

$$^i z_j = \frac{1}{^{c_i} z_j} \begin{bmatrix} ^{c_i} x_j \\ ^{c_i} y_j \end{bmatrix} + ^i n_j \quad (4.11)$$

where

$$^{c_i} p_j = \begin{bmatrix} ^{c_i} x_j & ^{c_i} y_j & ^{c_i} z_j \end{bmatrix}^T = C(q_w^{c_i})(p_w^j - p_w^{c_i}) \quad (4.12)$$

and $^i n_j$ is a zero-mean Gaussian measurement noise with covariance $^i R_j = \sigma_V^2 I_2$. Expressing the measurement model as a function of the state defines a nonlinear visual measurement function that can be represented as follows

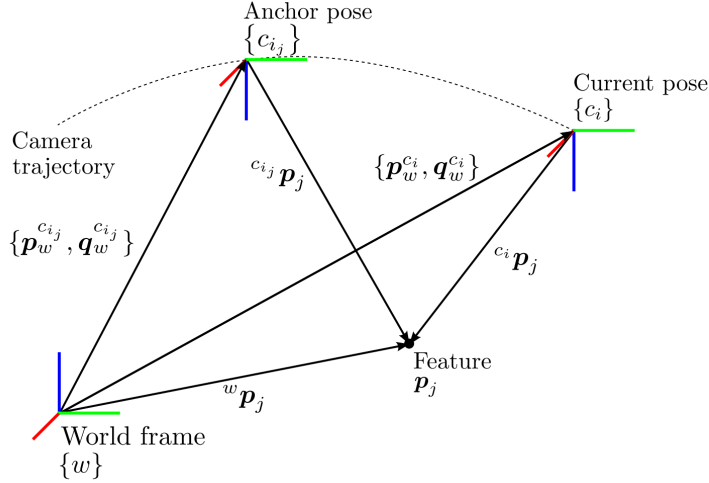


Figure 4.7: From [7], geometry of SLAM visual measurement of feature p_j observed in camera c_i , using inverse-depth parameterization with respect to anchor camera c_{ij} in the sliding window.

$$^i z_j = h(p_w^{c_{ij}}, q_w^{c_{ij}}, {}^w p_j) + {}^i n_j \quad (4.13)$$

The direct measurement of ${}^i z_j$ comes from any image point tracked over time by the visual front-end. In the context of range-feature initialization, the Cartesian coordinates of measurement p_{LRF_j} in world frame w and in turn camera frame c_i can be expressed as

$${}^w p_{LRF_j} = \begin{bmatrix} {}^w x_{LRF_j} \\ {}^w y_{LRF_j} \\ {}^w z_{LRF_j} \end{bmatrix} = p_w^{c_{i LRF_j}} + \frac{1}{\rho_{LRF_j}} C(q_w^{c_{i LRF_j}})^T \begin{bmatrix} \alpha_{LRF_j} \\ \beta_{LRF_j} \\ 1 \end{bmatrix} - q_w^{c_i} \quad (4.14)$$

$${}^{c_i} p_{LRF_j} = C(q_w^{c_i}) \left(p_w^{c_{i LRF_j}} + \frac{1}{\rho_{LRF_j}} C(q_w^{c_{i LRF_j}})^T \begin{bmatrix} \alpha_{LRF_j} \\ \beta_{LRF_j} \\ 1 \end{bmatrix} - q_w^{c_i} \right) \quad (4.15)$$

where $c_{i LRF_j}$ represents the anchor camera frame of feature p_{LRF_j} . The fundamental principle underlying this implementation is the expectation that the accurate depth information of a particular range feature should propagate through the covariance in the Extended Kalman Filter update. By doing so, it not only refines the estimation of that feature but also contributes to the overall improvement of other SLAM features.

An alternative strategy could involve reducing the value of σ_V applied to the range-feature update by a certain factor. This adjustment would essentially result in the EKF update assigning greater importance to the range-feature compared to the other SLAM features. Such a modification would prioritize the accuracy of the range-feature information, potentially leading to more substantial corrections and refinements in the estimation process.

Chapter 5

Experiments

This chapter of this thesis presents a comprehensive evaluation of key components crucial to the success of Mid-Air Helicopter Delivery in the Martian environment. The experiments are organized into three distinct blocks, each addressing critical aspects of the work done.

- The initial segment focuses on assessing the performance of the xVIO visual-inertial odometry framework on a single MAHD-like sequence by enforcing known initial conditions of the drone's state at run-time. This phase not only validates the quality of generated trajectories but also provides an initial evaluation of xVIO's suitability for MAHD.
- The second section explores the primary advantages of the implemented algorithm: on one hand the ability to observe scale without the constraints of a facet model assumption, one the other the vertical scale drift mitigation and overall improvements of the performance, highlighting its practicality in real-world MAHD scenarios.
- Finally, the third block extends the assessment into a Monte Carlo environment, comprehensively considering the different variables and uncertainties inherent to MAHD, such as sensor noise, trajectory variability, and environmental factors. These experiments collectively contribute to a thorough understanding of the proposed approach and its potential for enhancing the navigation and landing capabilities of the Mars Science Helicopter.

5.1 Sensor noise specifications

For all the experiments conducted, a consistent sensor setup was employed to ensure uniformity and reproducibility of results. The simulated IMU, reproducing the specifications of the *MPU-9250* Inertial Measurement Unit [10], features the following noise model parameters:

- Gyro noise spectral density: $0.0013 \text{ rad}/\text{s}/\sqrt{\text{Hz}}$
- Gyro bias random walk: $0.00013 \text{ rad}/\text{s}^2/\text{sqrt(Hz)}$

- Accelerometer noise spectral density: $0.0083 \text{ m/s}^2/\sqrt{\text{Hz}}$
- Accelerometer bias random walk: $0.00083 \text{ m/s}^3/\sqrt{\text{Hz}}$

The decision to use the *MPU-9250* IMU model in simulation, which is considered to be of lower quality compared to the *STIM300* [18] that will be deployed on the MSH, is a deliberate choice. This choice stems from the need to test the navigation system under more challenging conditions than those initially planned for MSH. By subjecting the navigation system to a more degraded scenario in the simulation, which includes the less accurate IMU model, you can account for potential vibrations and disturbances caused by the helicopter or jetpack during actual deployment. This approach allows for the creation of a safety margin or tolerance to accommodate these real-world challenges, ensuring that the navigation system can still perform effectively and robustly under adverse conditions.

As for the altimeter model utilized for these experiments, we simulate the *DLEM 30* Laser Range Finder, which incorporates a 1-meter standard deviation noise component on top of the true altitude value. *DLEM 30* is a high-precision Laser Range Finder that is able to measure targets up to several kilometers with sub-meter accuracy. In the specific case of the *DLEM 30*, the sensor has a measurement range from 10m to 14000 m with a resolution of 0.1 m. For simplicity, in the simulation the LRF is assumed to have the same origin as the camera frame at any time, even though in the real-world scenario there is a tiny translational difference between the two frames, that needs to be taken into account.

The camera model, integrated into the Unity simulation environment, featured a horizontal Field of View (FOV) of 90 degrees and generated images at a resolution of 640×480 pixels. This standardized sensor configuration provided a consistent basis for assessing the performance of the proposed algorithms across various experimental scenarios.

5.2 Framework validation with known state initial conditions

In this section, an assessment of xVIO’s performance is conducted using a MAHD-like trajectory generated within the Unity simulation environment. Notably, the visual-odometry framework is initialized with perfect knowledge of the initial state, in particular of the position, velocity, and attitude of the drone at time $t = 0$. This evaluation also incorporates the utilization of the implemented method for initializing range features. Several key parameters play a significant role in this assessment, including:

- Normalized feature noise standard deviation σ_V : This parameter represents the measurement noise associated with SLAM features updates. A lower value for σ_V results in greater trust in the SLAM feature updates by the Extended Kalman Filter.
- Feature tracker parameters: Parameters related to the feature tracker are crucial, including the window search size between adjacent frames and the

minimum eigenvalue error threshold for filtering out poor feature matches.

- Range-feature selection parameters: These parameters govern the initiation of new range features. Specifically, they include the minimum eigenvalue threshold required to trigger the addition of new features and the time interval to wait between triggering two consecutive range features.

Fine-tuning these parameters allows for a comprehensive evaluation of xVIO's performance under various conditions and scenarios, shedding light on its effectiveness within the context of MAHD.

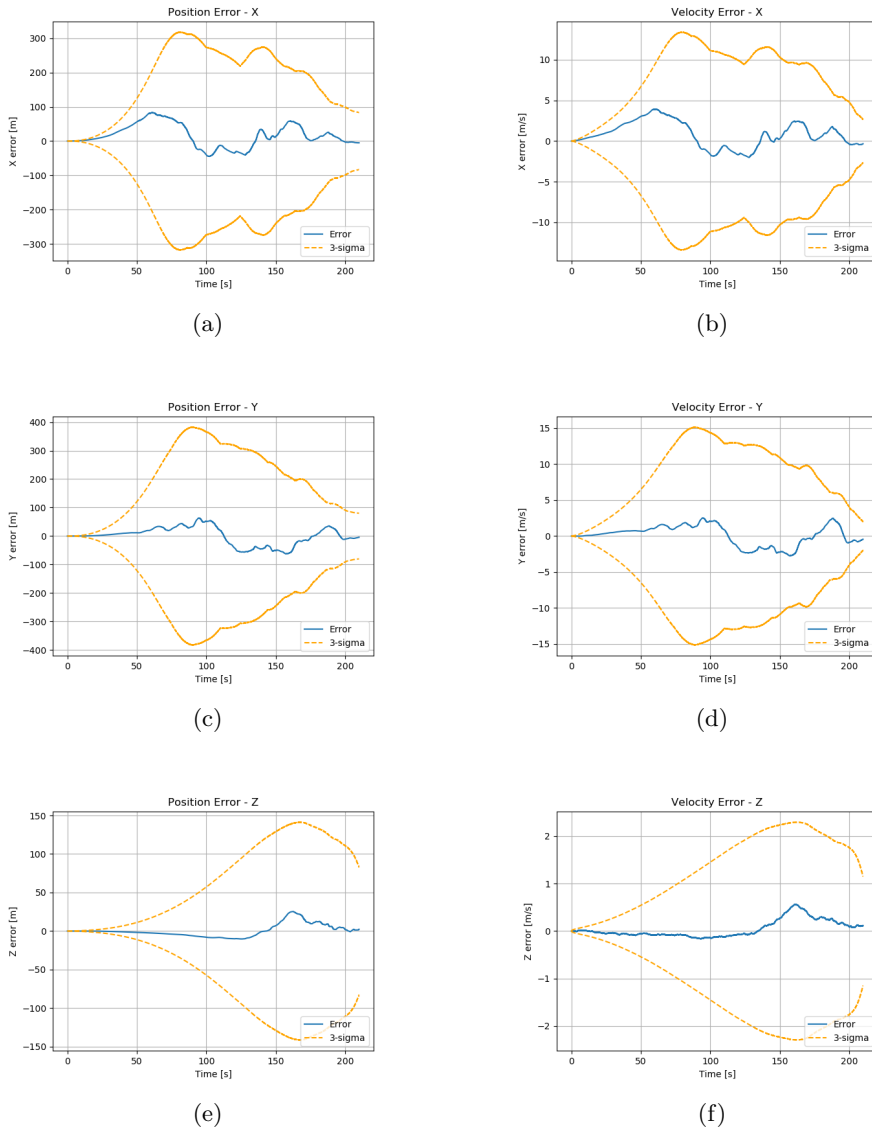


Figure 5.1: Position and velocity error plots of xVIO with range-feature initialization evaluated on a MAHD-like trajectory with known initial conditions.

Main points of discussion

The plots provide a detailed insight into the performance of the trajectory under consideration, which represents a descent trajectory starting from an initial altitude of 12 km above the ground. The drone's initial velocity is given as [-6, 10, -55] m/s, representative of the EDL trajectories for MAHD. These plots show the position and velocity errors throughout the trajectory, accompanied by 3σ uncertainty bounds.

The key observations from these plots are the following:

- The covariance, which indicates the level of uncertainty in the estimated states, is null at $t = 0$ as we are assuming to know perfectly the initial state of the system, but it gradually increases as the drone starts to move. This is expected since the accuracy of the estimated state diminishes over time due to the uncertainty and errors in the measurements and system model of the EKF.
- The covariance along the y-axis grows more rapidly than along the x-axis. This discrepancy is attributed to the fact that the drone's motion in the y direction has a higher degree of uncertainty compared to its motion in the x direction. This is due to the fact that the y component of velocity is larger than that of x, leading to increased uncertainty in the y direction.
- Given that the primary direction of motion is vertical (along the z-axis), the effect of range-feature initialization in mitigating scale drift is most evident in the z-axis plots. It is noticeable in Figure 5.1f that, after a small increase in error on the Z axis around time $t = 130$ s of the trajectory, the error is subsequently reduced to zero upon observing a range feature around time $t = 158$ s of the trajectory.

In summary, these plots offer a comprehensive view of how position and velocity errors evolve during the descent trajectory, showcasing the effectiveness of range-feature initialization, particularly in mitigating vertical drift, which is vital for the precision of the descent phase.

The analysis of this particular sequence reveals a favorable converging behavior of the estimator. Across all axes, we observe that the velocity estimation error remains within the specified 1 m/s 3σ boundaries. This outcome demonstrates that the performance requirements outlined in the MAHD specifications described in Section 1.3 are indeed met for this specific trajectory, however they need to be verified on a larger-scale analysis. The successful containment of velocity estimation error ensures that the mission concepts's objectives related to navigation and control are achieved within the desired parameters.

5.3 Evaluation of the range-feature initialization method

In this section, we will begin by demonstrating how the range-feature initialization method effectively resolves scale ambiguity. Subsequently, we will assess its performance in the context of more complex MAHD-like trajectories, highlighting the improvements it offers in such scenarios.

5.3.1 Scale observability with range-feature initialization

The primary objective of range-feature initialization revolves around testing the algorithm's effectiveness for scale observability. The trajectory employed for evaluation purposes takes a simpler form, characterized by a horizontal path featuring a velocity vector of $[50, 0, 0] \text{ m/s}$, staying the whole time at an elevation of 12 km above a uniformly flat terrain. This specific choice of trajectory was made to isolate potential effects arising from the 3D complexity of the environment.

The sequence is analyzed within the same analytical framework as previously described, although with the introduction of initial condition errors. Specifically, a 20% error is imposed upon the initial position, contributing to a perturbation in the scale aspect of the feature plane. Additionally, a 20% error is applied to the norm of the velocity vector, thereby establishing an overall scale error of 20%. With particular focus on the x-axis, representing the principal direction of motion, the results illustrated by the plots are noteworthy. In the absence of range-feature initialization, the scale factor remains unobserved.

However, a relevant transformation occurs after the initial triggering and incorporation of the first range-feature into the SLAM update process, an event that takes place at time $t = 61 \text{ s}$ (Figure 5.2a). It is important to highlight that within the framework of terrain-relative navigation, observation of the scale does not entirely nullify position errors, but it does lead to a reduction in velocity error to zero, as illustrated in Figure 5.2b. This outcome decisively underscores the algorithm's efficacy to observe the scale.

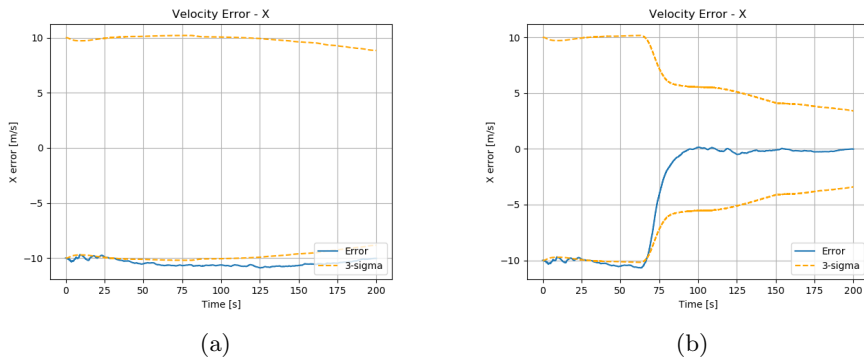


Figure 5.2: Comparison between position error on X (a) without and (b) with range-feature initialization. It is possible to observe how the effect of the range-feature, observed at time $t = 61 \text{ s}$, brings the velocity error to zero.

5.3.2 Improved performance on MAHD trajectories

This section serves as a more in-depth assessment within a single MAHD-like sequence, aiming to highlight the impact of range-feature initialization. The primary focus is on the velocity error along the z-axis, with a specific interest in observing the effectiveness of range-feature initialization in mitigating drift. In the trajectory under consideration, different from the one showcased before

in Section 5.2 the true velocity of the drone is $[-10, -1, -55] \text{ m/s}$, and the trajectory covers a range from 12 kilometers down to 200 meters.

Initialization with known state initial conditions

In this initial subsection, we assess the performance of xVIO with and without range-feature initialization. In both cases, we assume a known initial state of the drone. The primary focus is on comparing the velocity error along the z-axis, shown in Figure 5.3. While the error is relatively low in both scenarios, thanks to the perfect initial conditions of the estimator, it is important to point out that the 3σ covariance bound in the case of range-feature initialization is significantly narrower. This reduction in covariance bounds is not limited to the z-axis but also extends to the x and y axes. Deploying the range-feature initialization method allows us to reduce the final 3σ bounds on the velocity from $[1.264, 1.212, 3.740] \text{ m/s}$ to $[1.114, 0.961, 0.608] \text{ m/s}$. As long as velocity error plots on x and y are concerned, similar values are observed in both cases.

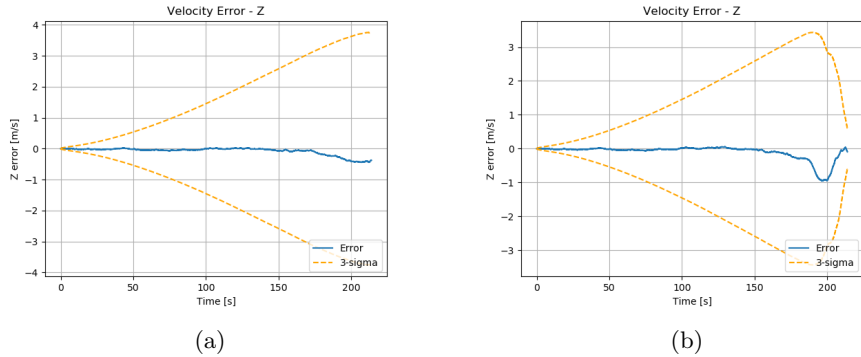


Figure 5.3: Comparison between velocity error on z axis (a) without and (b) with range-feature initialization method

Initialization under MAHD conditions

While the outcomes were quite similar while assuming perfect knowledge of the initial state, the true effectiveness of the novel algorithm becomes more apparent when dealing with the inherent randomness and complexities of MAHD. Further details regarding the initial evaluation conditions for real-world MAHD-like sequences will be provided in the Section 5.4.

In this case, while comparing the vision-only method to the one with range-features, we observe a divergence behavior in the velocity along the z-axis for the vision-only method. In contrast, Figure 5.4 shows that the range-features initialization approach consistently keeps the error close to zero throughout the entire sequence. This outcome serves as another validation of the effectiveness of the implemented method in challenging MAHD scenarios. Deploying the range-feature initialization method allows us to reduce the final 3σ bound on the velocity from $[1.613, 1.707, 3.653] \text{ m/s}$ to $[1.115, 0.983, 0.608] \text{ m/s}$.

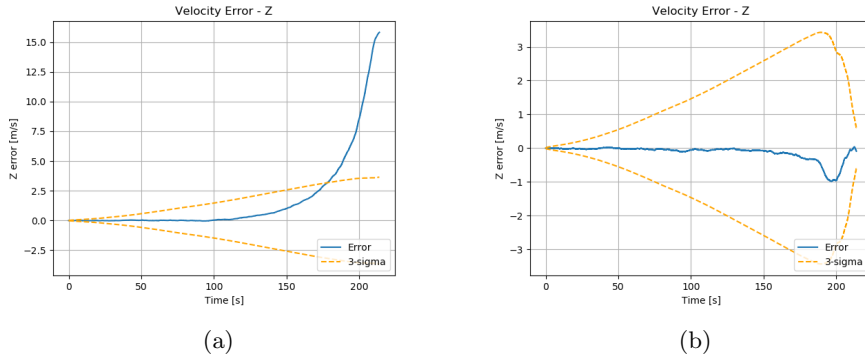


Figure 5.4: Comparison between velocity error on z axis (a) without and (b) with range-feature initialization method

5.4 MAHD Monte Carlo analysis

In this section, a Monte Carlo analysis is conducted to provide a more rigorous evaluation of the algorithm's performance within the context of the simulation environment. This approach enhances the robustness of the assessment by systematically considering various factors, including diverse trajectories, the influence of noise coming from the different sensors, and the incorporation of other possible uncertainties representative of real-life scenarios encountered during the deployment of the Mars Science Helicopter on Mars.

5.4.1 Experimental setup

In the scope of data generation, several key aspects undergo variation to create a rich and diverse dataset. Firstly, different trajectories are sampled within the environment, while ensuring both a consistent landing altitude of 200 meters above the ground and visibility of the 3D environment in the camera FOV at every step. Initial velocity parameters are perturbed, introducing a 45 m/s 3σ error exclusively to the x and y components due to lateral winds, with the z-component firmly set at the terminal velocity, directed downwards at approximately -56 m/s. Additionally, image noise, in the form of shot noise with a 1-pixel 1σ standard deviation, is injected into the simulated image data. The IMU and Laser Range Finder models adhere to previously outlined specifications, namely those of the 9 Degree Of Freedom *MPU-9250* IMU and of the *DLEM-30* altimeter, respectively.

On the evaluation front, further sources of uncertainty are introduced. The initial velocity provided during state estimator initialization remains fixed at $[0, 0, -56]$ m/s, despite the real value of the x and y velocities is different at each trajectory. An additional layer of complexity is introduced through the imposition of an initial attitude error, perturbing the true configuration by a 1 deg 3σ error across the x, y, and z axes. In addition to that, an error of the 20% on the true initial position of the drone is set at run-time. This Monte Carlo analysis seeks to analyze the algorithm's performance across a spectrum of real-world scenarios, providing invaluable insights into its reliability.

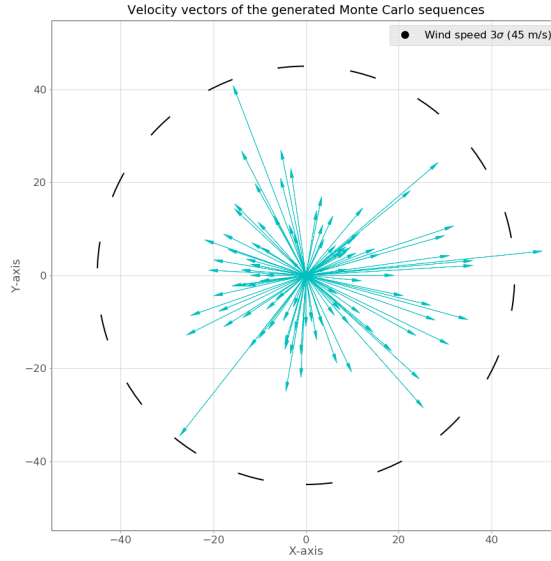


Figure 5.5: Velocity vectors of the generated sequences for the Monte Carlo analysis. The vectors represent the errors on the x and y components of the velocity due to wind. It has been observed that wind can add up to 45m/s 3σ velocity error on the horizontal components.

5.4.2 Results

Initially, a Monte Carlo evaluation will be conducted employing the xVIO framework with exclusively SLAM-based visual updates. Subsequently, the analysis will encompass the incorporation of the range-facet update model, followed by the activation of range-feature initialization. These sequential assessments will offer valuable insights into the system's performance across various configurations and functionalities.

For brevity, the plots we are presenting will focus solely on velocity, as it is the primary concern during the descent phase, crucial for jetpack control. The plots generated from the Monte Carlo analysis are organized in a vertical columnar layout. In the left column, the mean and standard deviation values for velocity errors along the x, y, and z axes are found, aggregated from the evaluation of all 100 trajectories. On the right side, there is a stacked view of the results for each individual trajectory, which facilitates the identification of potential outliers or variations across different trajectory instances. All the runs have been conducted with a value of $\sigma_V = 0.1$.

Evaluation of xVIO with only visual-inertial EKF update

The outcomes of the Monte Carlo analysis on xVIO with only visual-inertial update without range indicate that the model experiences divergence of the estimator in certain trajectories. The root cause of this divergence can be related to the wrong initial positioning of the drone, which is initialized with a 20% error. This initialization error might lead to a cascading effect on the estimation of the inverse-depths of each new feature during the SLAM features initialization process, ultimately leading to the divergence observed in some trajectories.

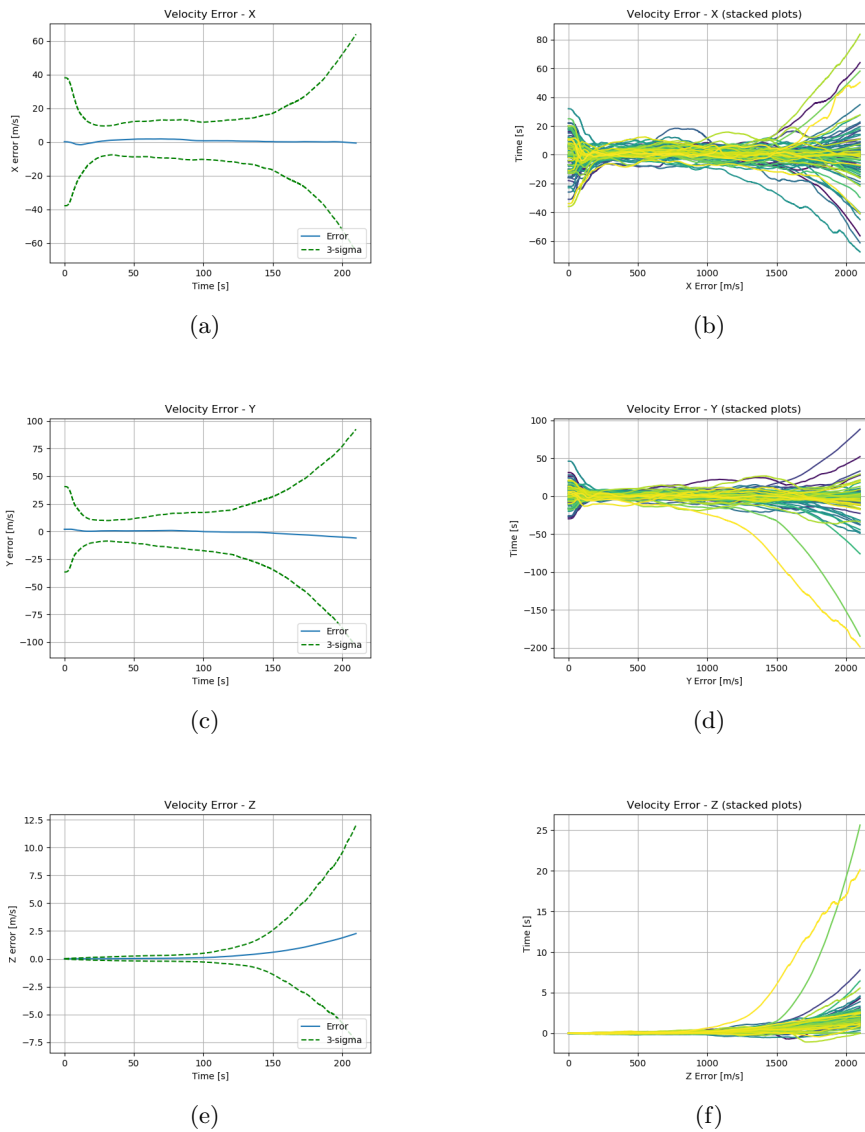


Figure 5.6: Velocity plots of the Monte Carlo analysis on 100 MAHD sequences generated on Unity and evaluated with xVIO with visual EKF update only.

Evaluation of xVIO with range-facet EKF update

The results from the Monte Carlo analysis, evaluated on xVIO incorporating the range-facet EKF update, reveal divergence in nearly all individual runs. This underscores the inefficacy of the method within the context of MAHD. The primary factor contributing to this inefficiency is the significant error associated with the local planarity assumption inherent in the method.

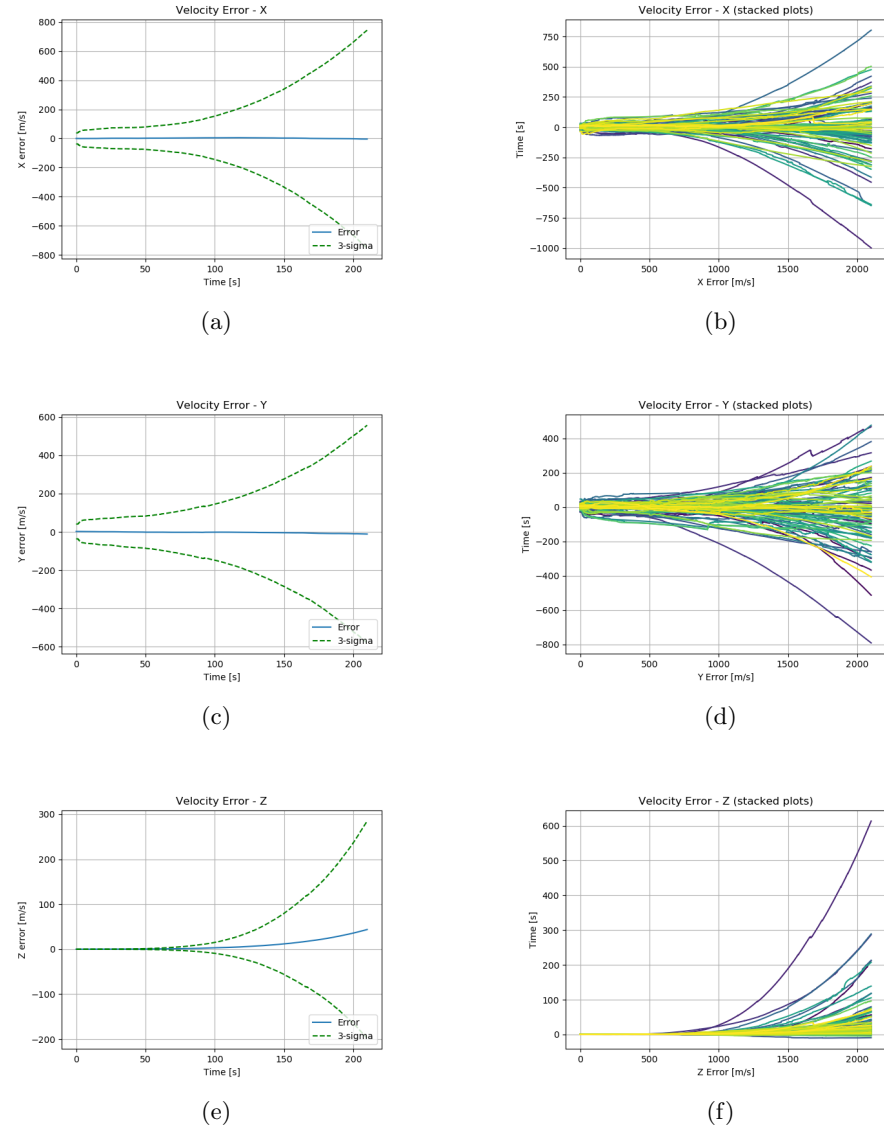


Figure 5.7: Velocity plots of the Monte Carlo analysis on 100 MAHD sequences generated on Unity and evaluated with xVIO with range-facet EKF update only.

Evaluation of xVIO with range-feature initialization

The Monte Carlo analysis evaluated on xVIO using the range-feature initialization method together with planar depth initialization with LRF measurements, demonstrates the method's superior performance among the three considered approaches. This outcome reaffirms the method's effectiveness in the context of MAHD.

It is important to note that the 20% error in the initial position does not have an impact on the range-feature initialization method in this particular run. This is because, in this specific scenario, we utilize planar depth initialization based on the LRF measurements. Consequently, the inverse-depth initialization of new SLAM features remains unaffected by any errors in the initial position, ensuring the robustness of the range-feature initialization process.

In contrast to xVIO with visual update only, when utilizing range-feature initialization, the state estimator does not exhibit divergence issues across any particular sequence. The chosen minimum eigenvalue threshold for this evaluation is $T = 0.01$. The overall results indicate that the mean velocity errors are centered around 0, while the final 3σ velocity bounds are as follows: [2.978, 2.686, 1.173] m/s. It is worth noting that these bounds slightly exceed the MAHD specifications described in Section 1.3 (velocity error contained within the 3σ 1 m/s bounds), mostly on the x and y axes.

Ablation study on the range-feature minimum eigenvalue threshold

In the subsequent Monte Carlo evaluation, we aimed to assess the impact of range-feature initialization, this time employing a lower minimum eigenvalue threshold of $T = 0.001$. The observed effects from the plots are largely comparable to the previous evaluation. However, it is worth noting that the final 3sigma value for velocity in the new evaluation has exhibited some variations, resulting in [3.162, 2.783, 0.892] m/s, as opposed to [2.978, 2.686, 1.173] m/s in the prior evaluation. This discrepancy can be attributed to the lower threshold, which leads to the inclusion of more range features in the tracking process. Consequently, the uncertainty along the z-axis decreases due to the increased number of features contributing. However, this also introduces a higher likelihood of incorporating less reliable features into the loop, resulting in slightly larger uncertainties along the x and y axes. This trade-off between feature quantity and quality manifests in the observed differences in the final 3σ values for velocity.

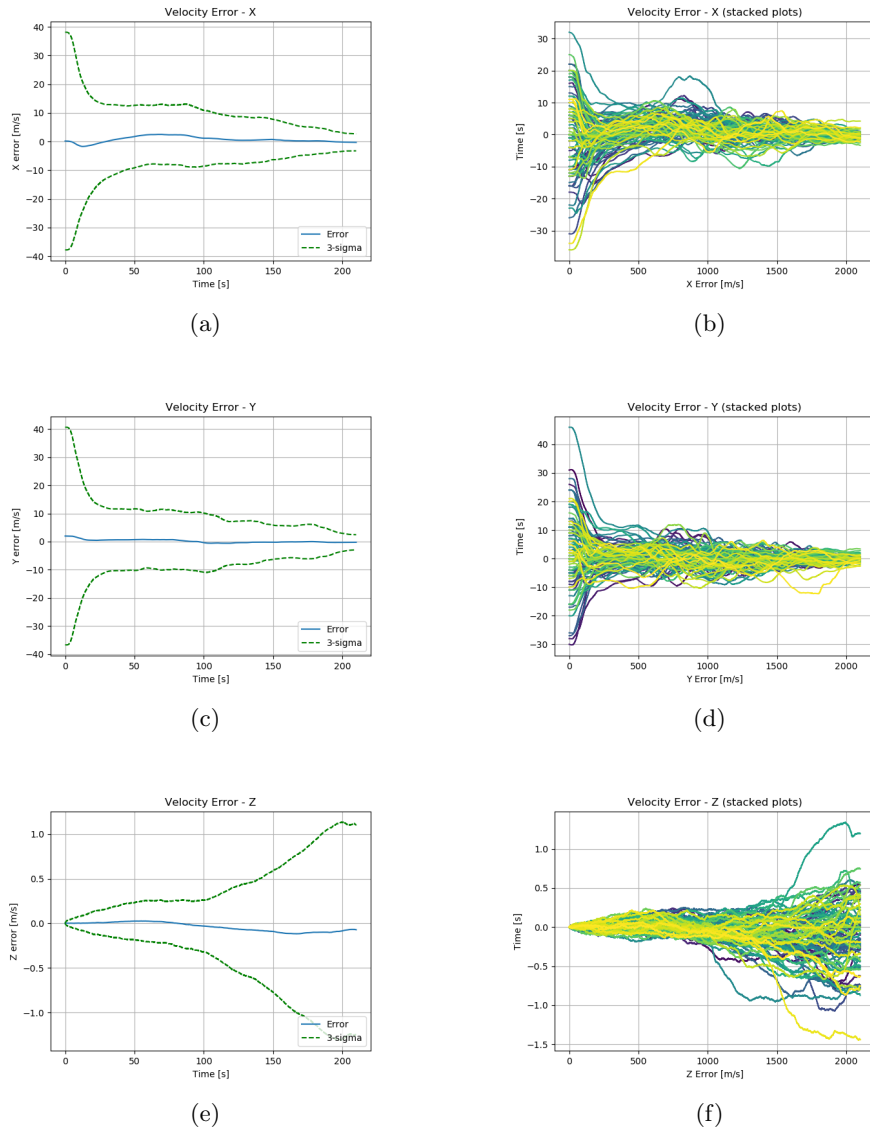


Figure 5.8: Velocity plots of the Monte Carlo analysis on 100 MAHD sequences generated on Unity and evaluated with xVIO with range-feature initialization and planar depth initialization with LRF measurement.

Chapter 6

Discussion

In the scope of this thesis, we conducted an extensive analysis of the range-VIO method, particularly focusing on its application in the challenging context of MAHD. Additionally, we introduced an innovative alternative approach to range-VIO that eliminates the necessity for ground planarity assumptions, making it adaptable to various terrain structures. This novel approach effectively maintains the capability to estimate scale and mitigate error drift during constant-velocity motion, all without relying on pre-existing maps. This research includes a comprehensive evaluation of the new implementation.

While we have showcased the method's advantages and its considerable performance enhancement when compared to xVIO relying solely on visual updates, the analysis has revealed that the velocity specifications set by MAHD are not entirely met in the spectrum of all the possible outcomes deriving from the Monte Carlo experiments. Consequently, there remains ample opportunity for further enhancement and refinement.

6.1 Conclusion

To summarize, the key contributions of this thesis can be outlined as follows:

- Development of a Mars-representative simulation environment.
- Design of an innovative range-feature initialization algorithm.
- In-depth analysis of the xVIO visual-odometry framework under the conditions envisioned for the MAHD mission concept.

One potential limitation of the implemented algorithm is its dependence on the texture of a single pixel when adding a range-feature. In certain types of environment with no such distinct textures, identifying a suitable feature to track along the whole trajectory can be challenging.

However, the inclusion of a new range-feature in the pipeline strictly depends on the value of the minimum eigenvalue threshold that is set at run-time. Balancing the range-feature minimum eigenvalue threshold in the context of terrains with poor texture is indeed a delicate task. On one hand, lowering the threshold can

be advantageous as it allows more range features to be considered, potentially improving the ability to estimate the scale in more texture-scarce environments. Nonetheless, it is crucial to strike the right balance because setting a threshold too low can result in the inclusion of bad matches. These inaccurate measurements can adversely affect the performance of the estimator, leading to issues such as performance degradation. Therefore, the choice of the range-feature minimum eigenvalue threshold should be made thoughtfully, taking into account the specific characteristics of the environment and the requirements of the application.

6.2 Future Work

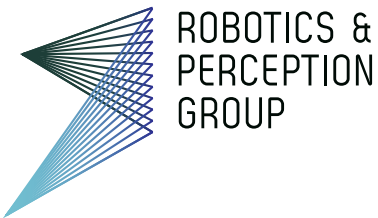
Looking ahead, the research will extend into several critical areas of investigation. One significant avenue we intend to explore involves assessing the performance of a delayed feature initialization block, which aims to enhance the initialization of SLAM feature depth. The goal is to enhance the accuracy of the MAHD trajectory by minimizing error during the initialization of other SLAM features depths.

Furthermore, we have plans to conduct comprehensive ablation studies on the implemented method. This will include evaluating the proposed framework on more intricate trajectories to gain a deeper understanding of its robustness and adaptability in diverse scenarios. In addition to simulated scenarios, we intend to validate the algorithm's performance in real-world operational conditions using collected data. These extensions will contribute significantly to expanding our knowledge of the algorithm's capabilities and identifying potential areas for optimization and refinement.

Bibliography

- [1] David S. Bayard, Dylan T. Conway, Roland Brockers, Jeff H. Delaune, Larry H. Matthies, HÅYvard F. Grip, Gene B. Merewether, Travis L. Brown, and Alejandro M. San Martin. *Vision-Based Navigation for the NASA Mars Helicopter*.
- [2] Paul A. Boeder and Carlos E. Soares. Mars 2020: mission, science objectives and build. In Carlos E. Soares, Eve M. Wooldridge, and Bruce A. Matheson, editors, *Systems Contamination: Prediction, Control, and Performance 2020*, volume 11489 of *Society of Photo-Optical Instrumentation Engineers (SPIE) Conference Series*, page 1148903, August 2020.
- [3] J.-Y. Bouguet. Pyramidal implementation of the lucas kanade feature tracker. 1999.
- [4] J. Civera, A. J. Davison, and J. Montiel. Inverse depth parametrization for monocular slam. *Trans. Rob.*, 24(5):932â945, oct 2008.
- [5] Javier Civera, Andrew J. Davison, and J. M. MartÃnez Montiel. Inverse depth parametrization for monocular slam. *IEEE Transactions on Robotics*, 24(5):932â945, 2008.
- [6] Peter Corke and Jesse Haviland. Not your grandmother's toolbox – the robotics toolbox reinvented for python. In *2021 IEEE International Conference on Robotics and Automation (ICRA)*, pages 11357–11363. IEEE, 2021.
- [7] Jeff Delaune, David S. Bayard, and Roland Brockers. xvio: A range-visual-inertial odometry framework, 2020.
- [8] Jeff Delaune, Jacob Izraelevitz, Samuel Sirlin, David Sternberg, Louis Giersch, L. Phillippe Tosi, Evgeniy Skliyanskiy, Larry Young, Michael Mischna, Shannah Withrow-Maser, Juergen Mueller, Joshua Bowman, Mark S Wallace, Havard F. Grip, Larry Matthies, Wayne Johnson, Matthew Keenon, Benjamin Pipenberg, Harsh Patel, Christopher Lim, Aaron Schutte, Marcel Veismann, Haley Cummings, Sarah Conley, Jonathan Bapst, Theodore Tzanatos, Roland Brockers, Abhinandan Jain, David Bayard, Art Chmielewski, Olivier Toupet, Joel Burdick, Morteza Gharib, J., and Balaram. Mid-air helicopter delivery at mars using a jetpack. 2022.
- [9] Bo Fu, Kumar Shaurya Shankar, and Nathan Michael. Radvio: Rangefinder-aided downward visual-inertial odometry. *CoRR*, abs/1810.08704, 2018.

- [10] InvenSense. Mpu-9250 product specification revision 1.1, 06 2016. Datasheet for the MPU-9250 IMU.
- [11] Junwoo Jang and Jinwhan Kim. Topographic slam using a single terrain altimeter in gnss-restricted environment. *IEEE Access*, 10:10806–10815, 2022.
- [12] Andrew Johnson, Seth Aaron, Johnny Chang, Yang Cheng, James Montgomery, Swati Mohan, Steven Schroeder, Brent Tweddle, Nikolas Trawny, and Jason Zheng. The Lander Vision System for Mars 2020 Entry Descent and Landing, 2017.
- [13] NASA / JPL-Caltech. Curiosity’s sky crane maneuver, artist’s concept, 2011. [Public domain; published October 3, 2011].
- [14] NASA / JPL-Caltech. Terrain relative navigation, 2021. [Public domain].
- [15] NASA / JPL-Caltech. What ingenuity and perseverance have discovered on mars so far, 2021. [Public domain; published November 17, 2021].
- [16] Dimitrios G. Kottas, Kejian J. Wu, and Stergios I. Roumeliotis. Detecting and dealing with hovering maneuvers in vision-aided inertial navigation systems. In *2013 IEEE/RSJ International Conference on Intelligent Robots and Systems*, pages 3172–3179, 2013.
- [17] NASA / JPL-Caltech Photojournal. Pia24729: Proposed mars science helicopter (illustration), 2021. [Public domain; published July 14, 2021].
- [18] Safran. Stim300. Datasheet for the STIM300 IMU.
- [19] Shital Shah, Debadeepta Dey, Chris Lovett, and Ashish Kapoor. Airsim: High-fidelity visual and physical simulation for autonomous vehicles. *CoRR*, abs/1705.05065, 2017.
- [20] Yunlong Song, Selim Naji, Elia Kaufmann, Antonio Loquercio, and Davide Scaramuzza. Flightmare: A flexible quadrotor simulator. *CoRR*, abs/2009.00563, 2020.
- [21] NASA / JPL-Caltech / Arizona State University. Valles marineris outflow channels mola zoom 64, 2013. [Source: JMARS; published February 16, 2013].
- [22] Yingxun Wang, Bo Shao, Chongchong Zhang, Jiang Zhao, and Zhihao Cai. Revio: Range- and event-based visual-inertial odometry for bio-inspired sensors. *Biomimetics*, 7(4), 2022.
- [23] Shannah Withrow-Maser, Wayne Johnson, Larry A. Young, Witold J. F. Koning, Winnie Kuang, Carlos A. Malpica, J. Balaram, and Theodore Tzanetos. Mars science helicopter: Conceptual design of the next generation of mars rotorcraft. 2020.
- [24] Kejian Wu and Stergios I. Roumeliotis. Unobservable directions of vins under special motions. 2016.



Title of work:

Vision-Based Navigation for Mid-Air Helicopter Delivery on Mars

Thesis type and date:

Master Thesis, October 2023

Supervision:

Jeff Delaune
Giovanni Cioffi
Prof. Dr. Davide Scaramuzza

Student:

Name:	Ivan Alberico
E-mail:	ialberico@student.ethz.ch
Legi-Nr.:	20-948-832

Statement regarding plagiarism:

By signing this statement, I affirm that I have read the information notice on plagiarism, independently produced this paper, and adhered to the general practice of source citation in this subject-area.

Information notice on plagiarism:

http://www.lehre.uzh.ch/plagiate/20110314_LK_Plagiarism.pdf

Zurich, 21. 1. 2024: _____